CHALMERS

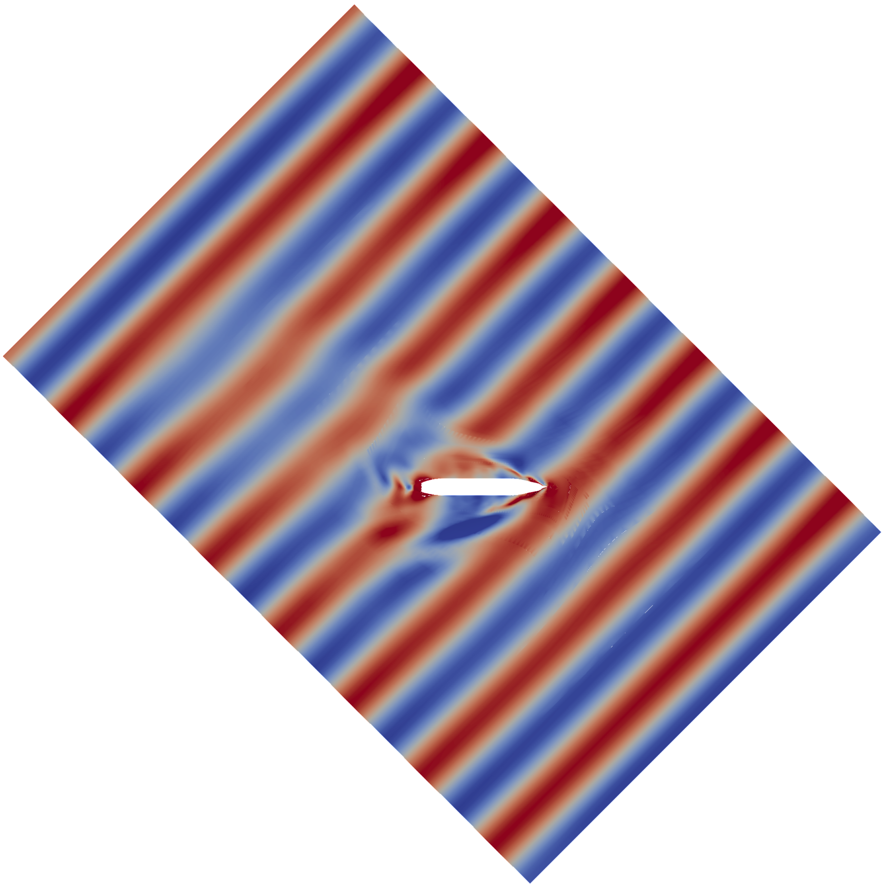

CFD Analysis of a Sailing Ship in Quartering Waves

Master's thesis in Applied Mechanics

RÉAN KREMER

Department of Mechanics and Maritime Sciences
CHALMERS UNIVERSITY OF TECHNOLOGY
Göteborg, Sweden 2020

MASTER'S THESIS IN APPLIED MECHANICS

CFD Analysis of a Sailing Ship in Quartering Waves

RÉAN KREMER

Department of Mechanics and Maritime Sciences
Division of Fluid Dynamics
CHALMERS UNIVERSITY OF TECHNOLOGY

Göteborg, Sweden 2020

CFD Analysis of a Sailing Ship in Quartering Waves
RÉAN KREMER

Master's thesis 2020:63
Department of Mechanics and Maritime Sciences
Division of Fluid Dynamics
Chalmers University of Technology
SE-412 96 Göteborg
Sweden
Telephone: +46 (0)31-772 1000

Cover:
Snapshot of the KCS sailing in bow quartering waves.

Chalmers Reproservice
Göteborg, Sweden 2020

CFD Analysis of a Sailing Ship in Quartering Waves
Master's thesis in Applied Mechanics
RÉAN KREMER
Department of Mechanics and Maritime Sciences
Division of Fluid Dynamics
Chalmers University of Technology

Abstract

Predicting the motions of a ship in waves has traditionally been done using methods based on potential theory. However, these methods are limited in the phenomena they can take into account and the level of information they produce. In these cases CFD can play an important role. In this report a CFD program called ReFRESCO is used to study the motion and force response of a ship sailing in regular quartering waves with 6 degrees of freedom. The ship in question is the KRISO container ship (KCS). First the necessary methodology is developed by incrementally increasing the number of degrees of freedom for a ship in bow quartering waves. The drift problem that is associated with surge, sway and yaw motion is solved by using conceptual spring models. Once a methodology is found, it is applied to a number of different cases with varying wave frequencies and amplitudes, both in stern and bow quartering seas. It is concluded that this method predicts the ship motion and surge force with reasonable accuracy. The forces in sway and yaw are also investigated, though no validation can be done as no experimental data is obtainable for comparison.

Keywords: CFD, Seakeeping, Ships

Preface

This report describes a 30 credit Master's thesis in the field of computational fluid dynamics and seakeeping. The project was carried out from February to July 2020 on behalf of the Maritime Research Institute of the Netherlands in order to establish a methodology for robust and fast CFD simulations of ships in both bow and stern quartering waves with 6 degrees of freedom. This is done by first establishing a methodology for a ship in bow quartering waves, before applying this to a ship in stern quartering waves.

MARIN senior researcher Stephane Rapuc together with MARIN CFD specialist Pierre Crepier were the industrial supervisors for the project and Professor Lars Davidson from the Division of Fluid Dynamics, Department of Mechanics and Maritime Sciences, Chalmers University of Technology was academical supervisor and examiner.

Acknowledgements

This project has been made possible with the help of several people that I would like to thank here. First I would like to thank everyone at MARIN for making my time at MARIN very enjoyable, and for putting in a lot of hard work to make it possible for me to continue my work despite the circumstances related to the pandemic. In particular I would like to thank Stephane Rapuc and Pierre Crepier for countless interesting and enlightening discussions, and for all their help and guidance during this project. Finally I would like to thank Professor Lars Davidson for his advice and help during the project.

Abbreviations

BC	Boundary Condition
CFD	Computational Fluid Dynamics
CoG	Center of Gravity
DoF	Degree of Freedom
KCS	KRISO Container Ship
KRISO	Korean Research Institute of Ships and Ocean Science and Technology
MARIN	Maritime Research Institute of the Netherlands
VoF	Volume of Fluid

Nomenclature

Symbol	**Unit**	**Designation**
B	m	Breadth
c	m/s	Celerity
D	N	Drag
F	N	Force
k	-	Stiffness constant
L	N	Lift
L_{pp}	m	Length between Perpendiculars
QTF	-	Quadratic Transfer Function
R	N	Resistance
RAO	-	Response Amplitude Operator
T	s	Wave period
Th	m kg / s^2	Thrust
V	m/s	Ship velocity
x	m	Displacement
β	deg	Heading
Δ	m	Draught
κ	1/m	Wave number
λ	m	Wave length
μ	Pa s	Dynamic viscosity
ρ	kg/m^3	Density
ω	rad/s	Frequency
ω_{e}	rad/s	Encounter frequency
τ	-	τ parameter

Contents

1 Introduction

In this chapter the background of the project, the project aim and the project limitations and objectives are presented and discussed.

1.1 Problem Background

Predicting the motion of a ship moving in waves has been a heavily researched topic in naval architecture since the inception of the field. Traditionally, this was done using methods based on potential theory, such as the strip method [1], the Green function method [2], the Rankine singularity method [3] and others. These methods have improved significantly over the years and are now capable of accurately predicting ship motions in a large number of cases.

However, despite these advancements, it is clear that there exist certain physical phenomena that can not be accurately taken into account by these methods, such as slamming and green water on deck, as well as certain forces that these methods cannot accurately predict. For these type of problems computational fluid dynamics (CFD) can play an important role [4]. Over the last years significant advancements have been made in both the available computing power, as well as in CFD as a whole. Moreover, CFD gives more detailed information on ships moving in waves than the traditional methods, as a result of the resulting information on the pressure and velocity fields that are inherent to CFD results.

Over the last decade many studies have been done both into problems that cannot be solved using potential flow solvers as well as into creating CFD programs that can not only match the accuracy of the predictions made by potential flow solvers, but even improve on it [5, 6, 7].

1.2 Thesis Goals

In this study, the motions of a ship in regular waves are investigated using a CFD program called ReFRESCO. The ship model in question is the KCS, which stands for KRISO container ship. The goal of this study is to find a methodology such that ReFRESCO can be used to provide an estimate of the motion and force response of a ship with 6 degrees of freedom (DoF) sailing in quartering waves within a reasonable simulation time. This prediction is not sought to be immensely accurate in this study; even rough correspondence between experimental work, a one dimensional solver and ReFRESCO results is enough to serve as a proof of concept. As a result, no turbulence models are included in the CFD simulations, as this would increase the required computational time greatly while not adding much for seakeeping.

When simulating a ship with 6DoF in quartering waves issues are expected to come up due to the complexity of such a system. To more easily isolate potential problems, several easier configurations are investigated before a fully free ship is considered. These configurations are designed in such a way that a relatively low amount of complexity is added between cases. As a result, any problems that are encountered can be isolated and solved separately. This makes for a structured approach for creating a methodology for the full 6DoF quartering system.

In particular the motions of the ship are initially investigated in head and bow quartering waves, rather than stern quartering waves. The reason for this is that a ship in stern quartering waves is significantly more complex than a ship in bow quartering waves. In order of complexity, the configurations that are to be investigated are:

- 2 DoF (heave and pitch) in head waves
- 2 DoF (heave and pitch) in bow quartering waves
- 3 DoF (heave, roll and pitch) in bow quartering waves
- 4 DoF (sway, heave, roll and pitch) in bow quartering waves
- 4 DoF (heave, roll, pitch and yaw) in bow quartering waves
- 5 DoF (sway, heave, roll, pitch and yaw) in bow quartering waves
- 6 DoF in bow quartering waves

- 6 DoF in stern quartering waves

The results from these cases are compared to experimental data and to the solutions of a Rankine source flow solver called FATIMA. From these comparisons, a conclusion is made about the validation of ReFRESCO for a sailing ship in quartering waves with 6DoF.

1.3 Scope

In this section the scope of this study is presented.

1.3.1 KCS

In this study the only ship that is taken into consideration is the KCS. This ship is especially created by the Korean Research Institute of Ships and Ocean Science and Technology (KRISO) for the purpose of CFD validation of a modern container ship with a bulbous bow. Experimental results have been generated before by using a scale model of this ship by e.g., Kim et al [8]. The experimental results used in this thesis however have been generated by MARIN and have yet to be published. Note that no full-scale KCS has ever been built. A numerical model of the KCS is shown in Figure 1.1.

Some important parameters of the KCS are given in Table 1.1 [9]. These values are inherent to the ship, and are therefore considered as given and unchangeable in this study. Here L_{pp} is defined as the length between the frontmost and backmost point of the ship at the waterline. B is the breadth and is defined as the width of the ship at the waterline. Δ is the draught and is defined as the length between the lowest point of the ship and the waterline. Finally, m is the mass of the ship.

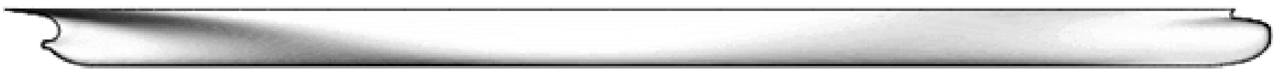

Figure 1.1: *A computational model of the KCS. The bow of the ship is on the right.[10]*

L_{pp} [m]	230
B [m]	32.2
Δ [m]	10.8
m [kg]	5.3×10^7

Table 1.1: Technical measurements of the KCS.

1.3.2 Sailing ship

In this study only a sailing ship, i.e. a ship moving at a constant significant forward speed, is considered. This means that, in calm water, the ship moves in the direction of the bow. In particular, the ship moves at 16 knots, which corresponds to 8.3 m/s. The reason that a sailing ship is considered, is because a ship that is standing still, or moving slowly, would present significant additional numerical challenges to the model. Moreover, a sailing ship is simply more realistic than one standing still when considering a ship in open water.

1.3.3 CFD

Since this study aims to validate the ReFRESCO CFD software for these kinds of simulations, only ReFRESCO is used to determine the ship motions. No other CFD codes are considered. No in depth study of the influence of parameter variation on the motions of the ship is done, though the model is tested for several wave frequencies and wave amplitudes. Taking only a small number of characteristic cases is enough to validate the CFD program.

The validation itself is done using experimental data. Furthermore, data generated using FATIMA is used. The wave frequencies and amplitudes are chosen such that experimental data is available for comparison.

However, for part of the solutions an experimental result is not available, due to the difficulty associated with measuring these parameters. There a comparison to only FATIMA is made. This makes the validation of ReFRESCO for these parameters more difficult, since FATIMA itself does not give perfect predictions. However, a comparison between ReFRESCO and FATIMA gives valuable information on the size and source of any errors that may be present. FATIMA, despite its assumptions, predicts the parameters that can be measured reasonably well. Moreover, it is simply the best solution available.

Finally, note that the data from experiments and FATIMA has already been generated. The details of these programs is only discussed insofar is necessary and relevant to the CFD results they are compared to.

1.4 Limitations

The main limitation in this study is the computational cost of the simulations. Due to the necessity of having a well defined surface boundary, the waves need to be clearly defined. As a result, a lot of cells are needed in the mesh. Even relatively simple cases with low DoFs and a coarse grid can take up to a full day to resolve on 200 cores. In other words, these kind of simulations require a high computational cost to run. As a result, well thought out choices need to be made regarding both the number of cases that are run, as well as how these cases are defined.

Another limitation is on the experimental results. These experiments have been done before this study began, and as such this study was not considered while choosing the different parameters corresponding to the different cases in the experimental work. As such, the choice of values for the different parameters in the computational cases is limited.

FATIMA is a 1D solver, which in and of itself brings a number of limitations when comparing to CFD solutions. The main one is that, in FATIMA, waves are of infinitesimal height. As a result it is not possible to study the influence of amplitude on the dimensionless solutions. Moreover, the same case that FATIMA considers can never be created using CFD, as CFD needs a finite wave height big enough to properly define with enough cells. This behaviour also needs to be taken into account when comparing between the two solvers. Moreover, the assumptions for FATIMA result in the FATIMA results being an upper boundary to the force response, rather than a good approximation, for sway and yaw.

2 Theory

In this chapter several key concepts related to CFD and seakeeping are explained. In particular some definitions and formula regarding waves and ship motions are discussed. Moreover, some general background information related to CFD, such as the Navier-Stokes equations, is provided. The conventions in which the ship response is usually expressed in the seakeeping community are also treated.

2.1 Computational Fluid Dynamics

CFD is the study of fluid flows using computer simulations. It is an important tool in seakeeping, where it is used to analyse how a ship interacts with the sea and air around it. A good understanding of this behaviour allows a naval architect to significantly improve on the design of ships in terms of efficiency and robustness. This could also be done using only experimental work. However, creating a good scale model is expensive and it takes a significant amount of time and effort to get useful experimental results. CFD is significantly cheaper and faster once a model has been validated. Moreover, CFD is more versatile, since small changes can easily be made to the ship without needing to revalidate the model, whereas in experimental work this would require the creation of a new scale model.

CFD can be divided into 3 steps: pre-processing, running of the simulation and post-processing. Pre-processing involves creating a mesh on the computational domain and setting the simulation settings. Running of the simulation involves letting a computer solve the governing equations of the fluid dynamics problem until the solution has converged within a certain preset tolerance for all time steps. For heavier CFD applications, like seakeeping simulations, this is done on a computational cluster rather than a PC due to the significant computer power needed to run these simulations within a realistic time frame. Finally, the post-processing step involves analysing the solution resulting from the simulation.

In this section the theory behind CFD is explained in terms of the governing equations. This is done only for parts that are relevant to the CFD simulations in this study. Finally, a short description of the CFD solver used in this study, ReFRESCO, is given.

2.1.1 Governing Equations

In seakeeping simulations the fluids in the domain are in general assumed to be incompressible. This is because ships move with a relatively low velocity and no significantly high temperatures or pressures are present in the flow field during a simulation. As a result, the governing equations of the simulations, comprising the equation of mass and the momentum equations, can be written in tensor notation as follows [11].

$$\frac{\partial v_i}{\partial x_i} = 0 \tag{2.1}$$

$$\rho \frac{\partial v_i}{\partial t} + \rho \frac{\partial v_i v_j}{\partial x_j} = -\frac{\partial P}{\partial x_i} + \mu \frac{\partial^2 v_i}{\partial x_j \partial x_j} \tag{2.2}$$

Equation 2.1 is known as the continuity equation and describes the transport of mass through the flow field. Equation 2.2 is known as the momentum equations and describes the transport of momentum through the flow field. Here the subscript $i = 1, 2, 3$ denotes the direction of the momentum transport corresponding to the x, y, z axis, respectively. Together they make up the Navier-Stokes equations. These can be supplemented by the energy equation, which describes the transport of heat through the flow field. Generally though, this is not done for seakeeping simulations since there are no significant temperature differences present.

To be able to solve these equations on a mesh they need to be discretized in both time and space. Discretization means that the equations are transformed in such a way that the derivatives are expressed in terms of the solutions of the neighbouring cells at the same iterations and the solutions at neighbouring cells and the same cell for previous iterations. There are many methods to do this, with significant difference in their efficiency, accuracy and robustness. In this study these will not be discussed, but the methods that are used are mentioned while discussing the numerical settings.

2.1.2 Multiphase flow

In seakeeping there are generally two fluids that play a role in the simulations: water and air. These two fluids are described by the Navier-Stokes equations described above, only with different values for density and viscosity. This generates a problem. If both fluids are solved by the same equations, then how does one ensure that the fluids stay separate while still allowing them to interact with each other? Moreover, it is possible for a single cell to be occupied by both air and water. How does one keep track of not only the percentage of air and water in a single cell, but also their respective position?

Over the years many methods have been proposed to solve this issue, with varying results. One of the most applied and generally accepted methods is called volume of fluid (VoF). In this method a parameter f is defined such that $f = 1$ in one of the fluids, e.g. water, and $f = 0$ in the other fluid, e.g. air. A transport equation can also be derived for this parameter. This transport equation is called the free surface equation and is given in Equation 2.3 [12] [13].

$$\frac{\partial f}{\partial t} + v_j \frac{\partial f}{\partial x_j} = 0 \tag{2.3}$$

This equation tracks the free surface of the fluids during the simulation. Density and viscosity also need to be adapted to ensure that the proper values in a cell are used in the Navier-Stokes equations. In these equations every cell is assumed to have a single value of density and viscosity associated with it. This is where f comes in, which is used to find an average value of density and viscosity over the cell, using the equations given in Equation 2.4 and 2.5. Here the angle brackets indicate an average over the volume of the cell [12] [13].

$$\rho = \langle \rho_1 f + \rho_2 (1 - f) \rangle \tag{2.4}$$

$$\mu = \langle \mu_1 f + \mu_2 (1 - f) \rangle \tag{2.5}$$

2.1.3 Turbulence

Turbulence also plays a minor role in seakeeping. However, in this study the choice has been made not to include a turbulence model in the CFD simulations. The reason for this is that no exact solutions are being searched for in this project. A rough agreement between the ReFRESCO solutions and the experimental results is enough to give confidence in the CFD software for these type of cases, and as such to validate it. This is possible with just a viscous flow simulation. While this introduces a minor error into the system, it also significantly decreases the complexity of the system.

2.1.4 ReFRESCO

In this study all results are generated using ReFRESCO [14]. ReFRESCO is a CFD solver developed by MARIN. It is an acronym, and stands for REliable and Fast Rans Equations (solver for) Ships (and) Construction Offshore. It is a state-of-the-art viscous-flow CFD code that is still under development even today, with the latest official update, 2.6.0, deployed in January of 2020.

One important aspect of ReFRESCO is that it employs a collocated grid. This means that all flow variables are stored at the same location. In all simulations throughout this thesis, the two fluids that are used are air and salt water. The corresponding material parameters for these fluids are given in Table 2.1.

	ρ [kg/m^3]	μ [Pa s]
Air	1.225	18.02E^{-06}
Salt Water	1026	1220E^{-06}

Table 2.1: Material properties of the used fluids.

2.2 Wave theory

When discussing the behaviour of a ship due to waves it is vital to first have at least a basic understanding of the different types of waves. The two main types are regular and irregular waves. Regular waves are the most simple. These are waves that are constant in time, with a pattern that is constantly repeated in the exact same way. One such regular wave shape is used in this thesis: the sinusoidal wave. This is a wave that has the same shape as a sine function [15].

Such a wave is depicted in Figure 2.1. Here the terms wave crest and wave trough are also shown. A wave crest is simply the part of the wave that is above the mean water height. Similarly, a wave trough is the part of a wave that is below the mean water height. A sinusoidal wave has, by definition, wave troughs and crests of equal length.

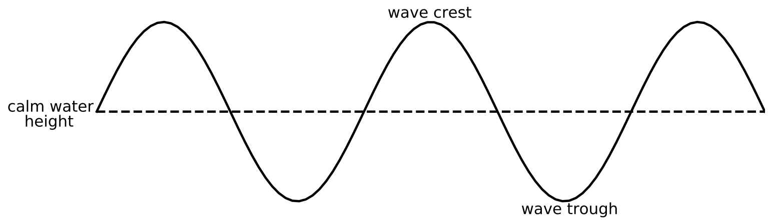

Figure 2.1: *Schematic of a regular wave. The dashed line is the water height in the absence of waves, known as the calm water height.*

Irregular waves consist of a large number of small regular waves compounded together. These small component waves all have their own wave height, wave length and direction. Irregular waves can be used to recreate any wave found in the ocean, by choosing the proper component waves. Because this study uses only regular waves, irregular waves will not be treated further here [15].

Regular waves are, in general, described by a time and a length parameter. The time parameter is either the wave frequency, ω, or the wave period, T. The length parameter is the wave length, λ, or the wave number, κ. The wave number and the wave period are defined in Equation 2.6 [16].

$$\kappa = \frac{2\pi}{\lambda}, T = \frac{2\pi}{\omega}. \tag{2.6}$$

These parameters can be used to calculate the celerity of a wave, c. The celerity is defined as the speed of a single wave trough or crest, and can be calculated using Equation 2.7.

$$c = \frac{\lambda}{T} = \frac{\omega}{\kappa}. \tag{2.7}$$

When considering a sinusoidal wave in deep water, Equation 2.8 holds, which relates the time parameter to the length parameter. Here g denotes the acceleration due to gravity.

$$\kappa = \frac{\omega^2}{g}. \tag{2.8}$$

Given the above equations, it is clear that a sinusoidal wave in deep water can be fully described using only the wave frequency and amplitude [16].

However, when considering a ship that is affected by these waves, another parameter is also important, namely the direction of the wave with respect to the direction of the ship. It is possible to give both the wave direction and the direction of the ship in absolute terms, i.e., as a function of the coordinate system. However, since only the direction with respect to the other is of importance, the wave direction is generally defined relative to the ship direction, see Figure 2.2. The angle between these two directions is called the wave heading, and is denoted by β.

It is also important to realize that the frequency of the waves is not the same frequency at which the ship will be affected by the waves when the ship is travelling at a non-zero velocity. The encounter frequency is thus defined, denoted by ω_e. This is the frequency at which the ship is affected by the waves. The encounter frequency is given in Equation 2.9 [16].

$$\omega_\mathrm{e} = \omega \left| 1 - \frac{\omega V}{g} \cos\beta \right|. \tag{2.9}$$

From this equation it becomes clear how the ship is affected by bow quartering waves and stern quartering waves. Bow quartering and stern quartering refer to cases with heading equal to 135 and 45 degrees, respectively. This means that in bow quartering waves the encounter frequency is higher than the wave frequency, while in stern quartering the opposite is true.

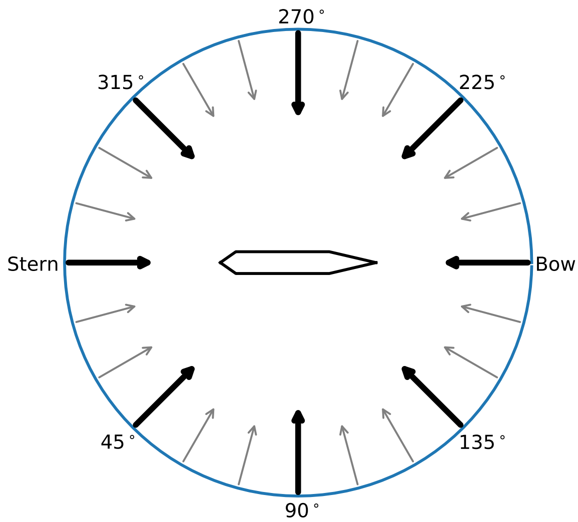

Figure 2.2: *Schematic of the wave direction with respect to the ship position.*

Finally, it is important to note that the velocity of a group of waves excited in calm water is not the same as the wave velocity. The reason for this is that the waves at the front of the group will decay, whereas at the back new waves will be formed. This results in a lower group velocity compared to the wave velocity. In particular, it turns out that the group velocity is equal to half of the wave velocity [16].

2.3 Radiated waves

When modelling a ship in waves it is important to ensure that any reflections from the boundaries of the computational domain do not influence the ship response. These reflections are caused by waves radiated from the ship. The radiated waves move from the ship to the boundaries of the domain. If they are not fully absorbed there, they will travel back towards the ship and influence the response.

However, when the ship is moving at a forward speed, it is possible that the waves are left behind and thus never reach the ship after radiation. To determine whether this is the case, the τ parameter should be calculated, the definition of which is given in Equation 2.10. This parameter relates the encounter frequency to the ship speed [17].

$$\tau = \frac{\omega_e V}{g}. \tag{2.10}$$

Through this parameter, four distinctive regions can be identified. The behaviours of these regions are sketched in Figure 2.3. Here it is clear that for τ larger than 0.25, the radiated waves are completely left behind by the ship. This means that in this case, the reflections of the radiated waves do not need to be considered in the analysis, as they are left behind by the ship and thus cannot influence the ship response. For τ smaller than 0.25 the radiated waves do need to be taken into consideration.

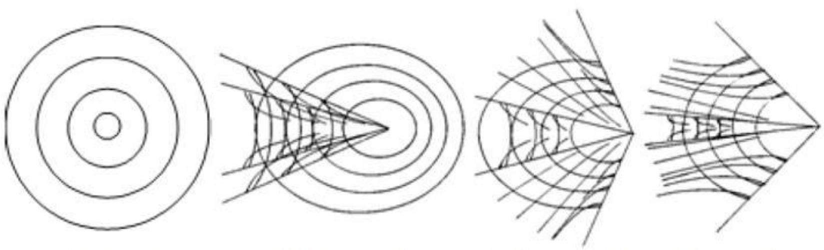

Figure 2.3: *Sketch of the wave propagation direction for different values of τ. [18]*

2.4 Wave added resistance

The wave added resistance is the resistance on a ship due to the presence of waves in the path of the ship. This is independent of the resistance caused by the water due to the forward motion of the ship, the so-called calm water resistance. The wave added resistance is an effect that has been studied in depth over the last years, because it plays such a dominant role in the ship response to waves [19, 20].

The wave added resistance is difficult to measure directly, even numerically. However, for a ship in waves moving at a forward speed, the resistance from the waves and the calm water resistance are dominant. As a result, the wave added resistance can be approximated by taking the difference between the total resistance on the ship and the calm water resistance, as shown in Equation 2.11.

$$\overline{F}_{\text{Waves}} = \overline{F}_{\text{Total}} - F_{\text{CW}}. \tag{2.11}$$

In Equation 2.11 it can be seen that the mean of the force is used, rather than the instantaneous value. The reason for this is that the resistance due to a wave is not constant in time, but rather changes over the duration of a wave. To determine the effect of waves it is thus necessary to average the forces over an integer number of waves. For the calm water resistance this is not the case, because this force is constant, assuming that the speed of the ship is constant.

2.5 Degrees of Freedom

In the seakeeping community, the response of ships due to the influence of waves is typically treated in a 6DoF system. This means that the motion of a ship is described in six parameters, divided into two groups of three. The first group describes the ships translational motion, and the second group describes the ships rotational motion.

The translational motion of the ship is easily described in terms of the axes of the computational domain, i.e., the ship motion is expressed in terms of the translation of the ship along the x, y and z-axis. These motions are called surge, sway and heave, respectively. Here the x-axis is defined to be in the direction that the ship is facing, while the z-axis is pointing straight up. Looking in the positive x-direction, the y-axis is defined to be to the left.

Similarly, the rotational motion of the ship is also described in terms of the computational axes. In this case though, the motion is defined as rotation around a principal axis. This gives the second group of three parameters, the rotation around the x, y and z-axis. These are called roll, pitch and yaw, respectively. The possible motions of the ship are sketched in Figure 2.4.

2.6 RAO and QTF

In order to more easily compare results from different ships and waves, the motions of the ship are normalized using the wave amplitude, as is convention for seakeeping. This results in a parameter known as the response amplitude operator (RAO). It is defined as translational or rotational motion over the wave amplitude, see Equation 2.12.

$$RAO = \frac{A}{A_{\text{wave}}}. \tag{2.12}$$

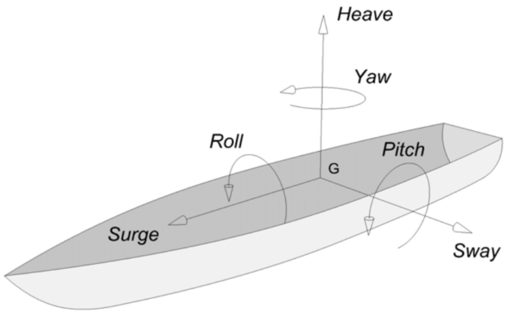

Figure 2.4: *Schematic of the degrees of freedom of a ship. [21]*

Here A is the amplitude of either surge, sway or heave motion, resulting in a non-dimensional RAO, or roll, pitch or yaw motion, resulting in an RAO with units deg/m.

Such a definition works well for motions with zero mean displacement, but this is not always the case in this study. Therefore, instead of doing a harmonic analysis with respect to 0, a harmonic analysis with respect to a moving average is done. The moving average at a point is defined to be the average of half an oscillation before, and half an oscillation behind the point. This ensures that the amplitude of the motion caused only by the wave is found and thus that larger scale motions are not taken into account.

The wave added resistance describes, together with the RAO, the response of the ship to the waves. Since the motions have been made independent of the amplitude, this is done with the resistance as well. The resulting parameter is called the quadratic transfer function (QTF). The QTF is a measure of the force in the direction of the corresponding DoF. It is defined as in Equation 2.13. In this equation the definition is given in terms of forces for the translational DoFs. The definition for the rotational DoFs is analogous, with moments instead of forces.

$$QTF = \frac{\overline{F}_{\text{WA}}}{A^2_{\text{wave}}} = \frac{\overline{F}_{\text{total}} - F_{\text{CW}}}{A^2_{\text{wave}}}. \tag{2.13}$$

It should be noted that the calm water added resistance for sway, roll and yaw is 0. This is because the ship is symmetric and moving along the x-axis. In those cases, the QTF can be denoted as shown in Equation 2.14. QTF has units of N/m^2 for the forces, and units of Nm/m^2 for the moments.

$$QTF = \frac{\overline{F}_{\text{total}}}{A^2_{\text{wave}}}. \tag{2.14}$$

3 Research Methodology

In this chapter the process that was used to generate numerical results in this study will be explained in detail. First the meshing strategy is discussed. Secondly the setup of the simulations is treated. Then the details of the different cases considered in this study are explained and quantified. Finally some remarks about the analysis are made.

3.1 Meshing Strategy

In this section the meshing generation is discussed. It is assumed that a valid STL file for the KCS is available. In this file exactly half of the ship and the domain should be defined. The mesh generation is done using a program called HEXPRESS (version 8.2), developed by Numeca [22]. HEXPRESS is a program that generates hexahedral unstructured meshes. A mesh is said to be sufficient for use in ReFRESCO if all cells conform to the following guidelines:

- No negative cells
- No concave cells
- No twisted cells
- Minimum orthogonality should be 20 degrees or higher.
- Maximum equiangular skewness should be 0.90 or lower.

Note that the aspect ratio is not mentioned here, even though it is in general an important parameter to consider when determining the quality of a mesh. The reason for this is that ReFRESCO is very robust in terms of the aspect ratio, and can get good results no matter what the aspect ratio is. Therefore the meshes used in this study generally have high values of the aspect ratio, as that generally corresponds to a lower number of cells.

3.1.1 HEXPRESS

In HEXPRESS the mesh is generated through the following five separate steps:

1. Mesh initialization
2. Mesh adaptation
3. Snapping onto geometry
4. Optimization
5. Viscous layer insertion

In this subsection these steps are discussed in detail.

1. Mesh initialization

In this step a rough structured cubic grid is generated that spans the entire computational domain. This includes the ship volume, which is ignored for now. This grid is called the initial mesh, and it consists of the largest cell size possible in the final mesh. The final grid is achieved by splitting these cells into multiple smaller cells.

The length of the cubes in the rough grid is fully dependent on the length between perpendiculars (L_{PP}) of the ship. The length, width and height of the domain are defined as an integer multiplication of L_{PP}. Therefore, the length of the cubes can be chosen in such a way that an integer number of cells, usually 5 to 7, have a combined length equal to L_{PP}. This means that an integer number of cells precisely fills up the computational domain. An example of such an initial mesh is shown in Figure 3.1. Here the red line in the middle denotes the outline of the ship, and it is clear that it intersects with the mesh.

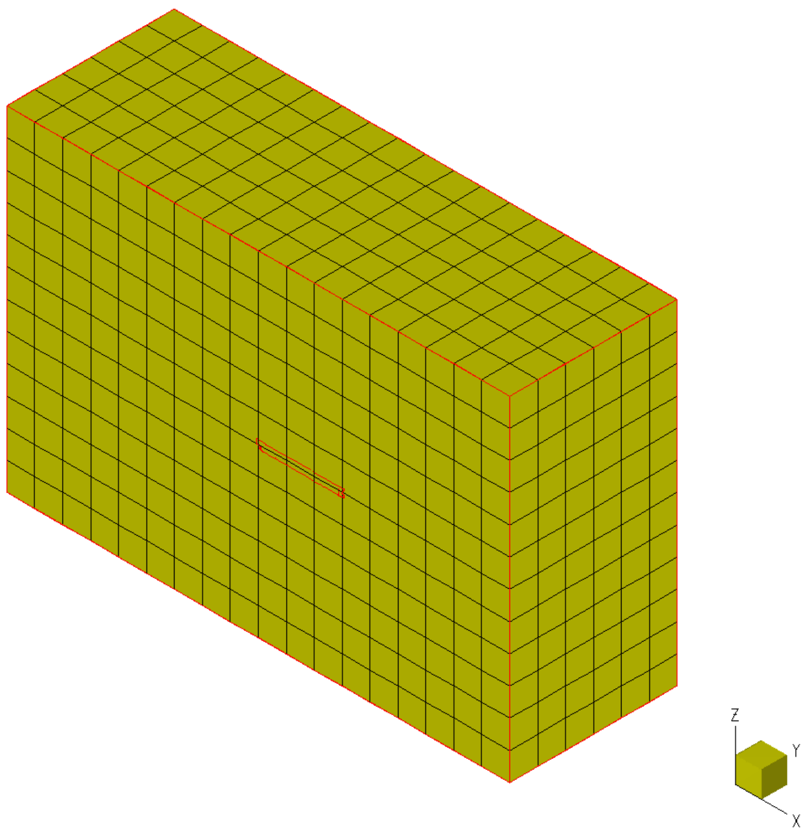

Figure 3.1: *Initial mesh for the domain of a half ship.*

2. Mesh adaptation

The next step is mesh adaptation. Here the mesh is made finer in areas where it is necessary, while sticking to the initial cell size in areas where it is not. This is done through a process called cell splitting. In this process a cell is made smaller by splitting it in half in one or more directions, see Figure 3.2. Since the aspect ratio does not matter for ReFRESCO, every direction can be split independently.

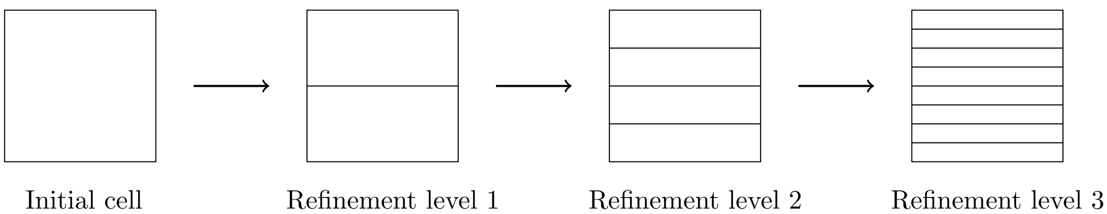

Figure 3.2: *Refinement levels as used in HEXPRESS for a single direction.*

The cells do not need to be split the same amount of times everywhere in the grid. The level of refinement, the amount of times a cell needs to be split, is set by using boxes. These boxes encapsulate a part of the domain, and are associated with a preset level of refinement as well as a target cell size in all three directions. The cells within these boxes are then refined in a direction until the cell size in that direction is below the target cell size, or until they are split an amount of times equal to the maximum refinement level of the box. If two boxes overlap, the highest refinement level is used.

This method leads to large discontinuities at the edge of boxes with high refinement levels. To resolve this, a diffusion parameter is defined. This sets the least amount of cells that a certain refinement level needs to have, before the cells next to it are allowed to be of a higher or lower refinement level. Throughout this study a global diffusion parameter equal to 1 is used.

In this study the cases are all quite similar in terms of the mesh. This means that the same boxes are used throughout, unless otherwise indicated. An example of these boxes are given in Table 3.1, together with the corresponding maximum refinement level and the target cell sizes. The positioning of the waves boxes is based on previous research[23]. In the table it stands out that only two target cell sizes are used, 1000 m and 0. A target cell size of 0 in a certain direction means that the cells in that direction should be refined until the maximum refinement level is reached. Conversely, a target cell size of 1000 m indicates that the cells do not need to be refined in that direction, since the target cell size is larger than the cell sizes in the initial mesh. Snapshots of the different boxes are shown in Figures 3.3 and 3.4.

If a mesh is created for a range of frequencies or amplitudes, several extra boxes could be defined. This is to ensure that the waves are properly defined over the entire range of parameters. As a results these boxes have a slightly different refinement level and slightly different size. In particular at the free surface an extra box is usually added, as the wave height and frequency are dominant in the box positioning there.

Box Name	Maximum Refinement Level	Target Cell Size [m]		
		x-axis	y-axis	z-axis
Ship box	6	0	0	0
Fore Ship Waterline box	9	1000	1000	0
Aft Ship Waterline box	8	0	0	0
Air Volume Fraction box	8	1000	1000	0
Upper Wave Length box	3	0	1000	0
Lower Wave Length box	2	0	1000	0
Ship Free Surface box	8	1000	1000	0
Close Ship Wave box	4	0	0	0
Medium Ship Wave box	3	0	0	0
Large Ship Wave box	2	0	0	0
Deep Large Ship Wave box	1	0	0	0

Table 3.1: Definition of the refinement boxes and their parameters for a bow quartering mesh corresponding to waves with $f = 0.575$ rad/s and $A = 0.75$ m.

Finally a maximum refinement is placed on the surfaces of the ship, with a target cell size in all three directions equal to 0. This ensures that the cells next to the walls are suitably small. This is important, because problematic cells in terms of the orthogonality usually appear adjacent to the walls. This also gives the user a good tool to fix any issues near the walls, without resulting in a significant increase in number of cells. The maximum refinement of these surfaces is given in Table 3.2. Figure 3.5 illustrates the placement of these surfaces on the ship.

Surface	0	1	2	3	4	Deck	Transom
Maximum Refinement Level	8	7	6	7	8	6	7

Table 3.2: The surfaces of the ship and their corresponding refinement level.

3. Snapping onto geometry

In this step the mesh is adapted in such a way that the ship geometry is excluded from the computational domain. First all cells whose volume is entirely inside of the ship, and thus completely outside the computational domain, are deleted. This leaves a mesh which roughly follows the shape of the ship, but still includes cells that pierce the ship geometry. To deal with these cells, the mesh is deformed by stretching, turning and trimming of cells, until the mesh no longer includes any part of the ship geometry.

4. Optimization

The previous step may lead to problematic cells, e.g., negative cells or cells with low minimum orthogonality. In this step these cells are dealt with by removing or modifying them.

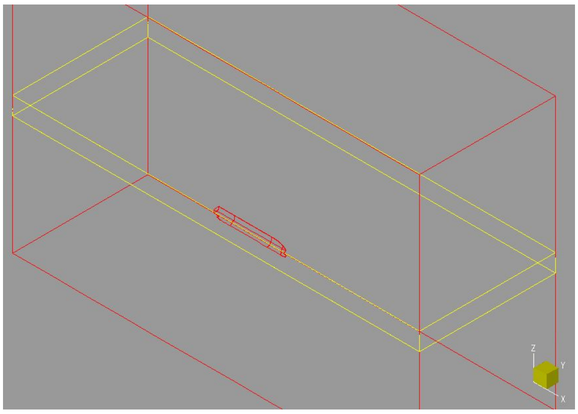

(a) *Upper Wave Length Box*

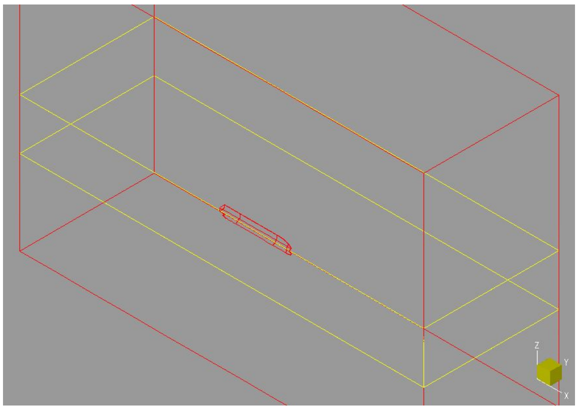

(b) *Lower Wave Length Box*

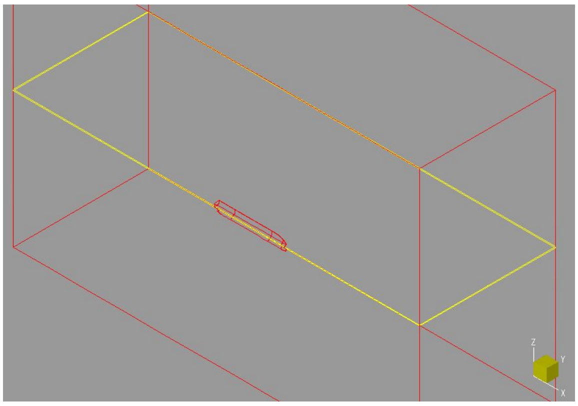

(c) *Air Volume Fraction Box*

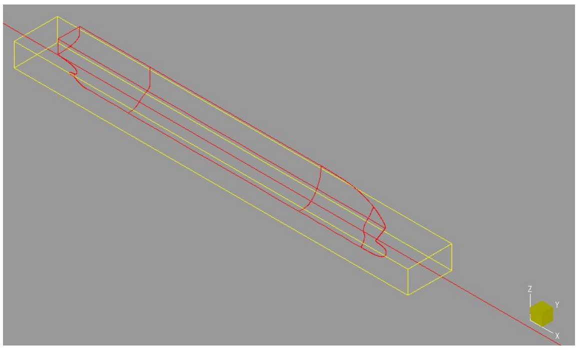

(d) *Ship Box*

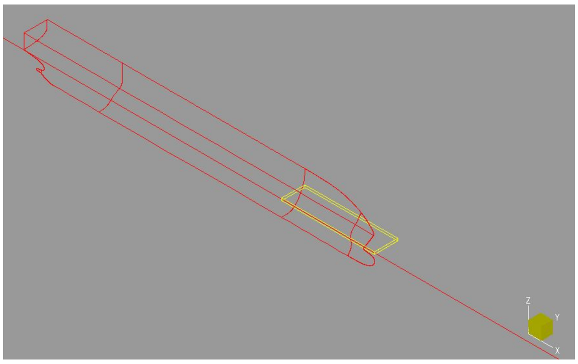

(e) *Fore Ship Waterline Box*

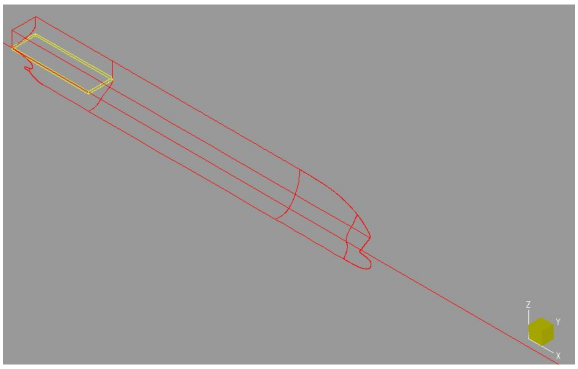

(f) *Aft Ship Waterline Box*

Figure 3.3: *Snapshots of a number of boxes used to create the mesh.*

5. Viscous layer insertion

Finally further refinement near the ship is necessary in order to properly capture the viscous effects. This is done by splitting the cells close to the walls, creating boundary layers. Where necessary the cells near the walls are modified to avoid problems with the cells in the newly formed boundary layers. A size of 0.01 m is chosen for the first boundary layer cell. The number of boundary layer cells is then calculated automatically based on the y^+.

3.1.2 Finalizing the mesh

For a ship in head waves, the meshing strategy as described above is sufficient to generate the mesh. The fact that only a half ship is considered is then taken into account by using a symmetry BC in ReFRESCO. In this

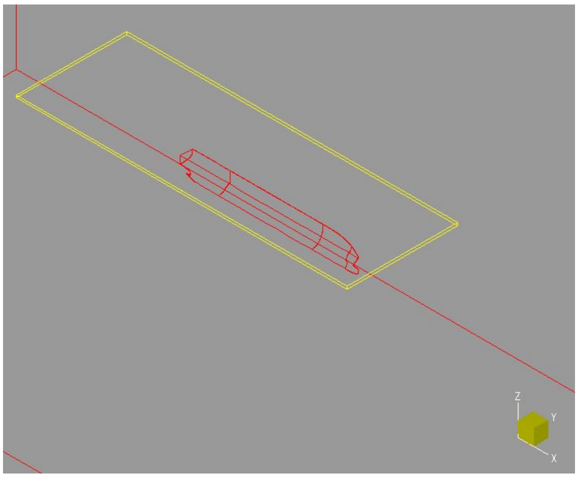

(a) *Ship Free Surface Box*

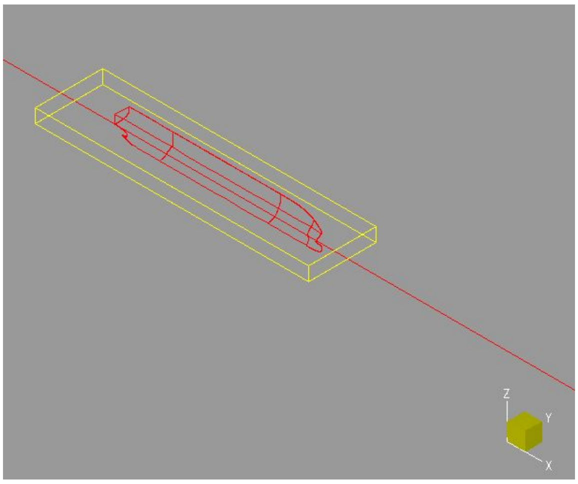

(b) *Close Ship Wave Box*

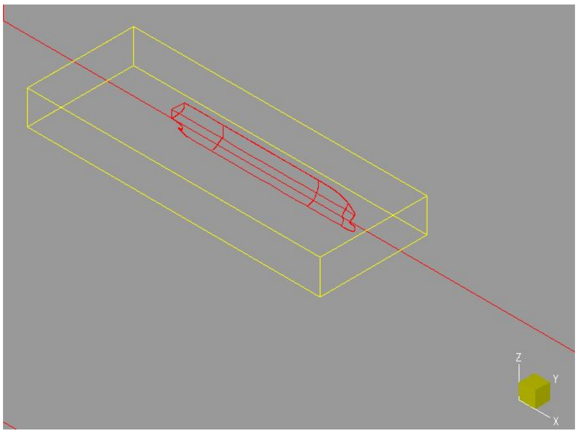

(c) *Medium Ship Wave Box*

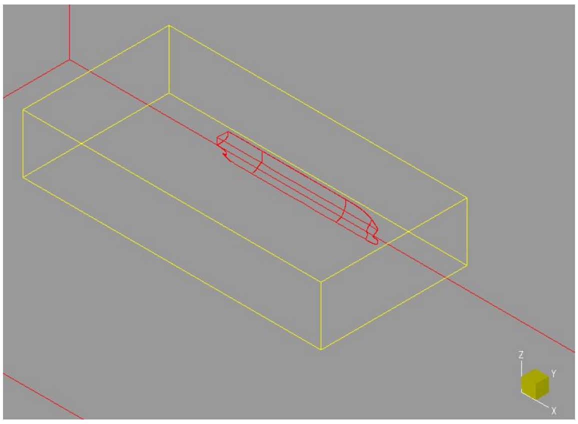

(d) *Large Ship Wave Box*

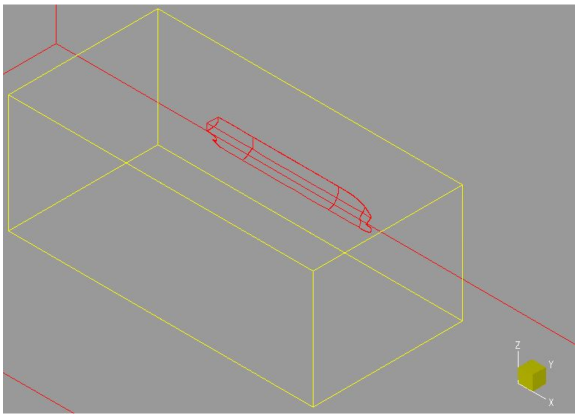

(e) *Deep Large Ship Wave Box*

Figure 3.4: *Snapshots of a number of boxes used to create the mesh.*

case it is possible to split the cells only in the x and z-direction for the cells that are not close to the ship. The reason for this is that the wave is coming into the domain exactly in the minus x-direction. As a result nothing is happening in the y-direction in the area that is not near the ship. Not splitting the cells in even a single direction saves a tremendous amount of computational time, since the total number of cells in the mesh is significantly smaller as a result.

However, for quartering waves this is more complex. Firstly, it is necessary to make a mesh that spans the

Figure 3.5: *Sketch of the surfaces on the KCS. The thick green and blue line correspond to the deck and transom of the ship, respectively.*

full domain, as it is not possible to use a symmetry BC in this case. The reason for this is that quartering waves are moving in both the x and the y -direction, so there are significant non-symmetrical physical effects at play. Additionally, if the mesh was generated in the exact same way as above, then the waves would enter the computational domain at one of the corners. The cells would thus no longer point in the same direction as the wave is travelling. Both phenomena result in significant decreases in accuracy compared to otherwise equal meshes.

There are two ways to fix this problem. The first is to accept that the cells are not in the same direction as the waves. In order to decrease the resulting errors to an acceptable level, it is necessary to employ grid refinement in both the y-direction and in the x-direction. For quartering waves the grid refinement factor would be the same in both directions. This leads to a significant increase in the total number of cells, and thus in computational time necessary to run a simulation with such a mesh.

In order to keep the computational time to an acceptable level the second method is employed in this study. First a mesh is created in the same way as was done above for the head waves, i.e. only grid refinement in the x and z-direction is considered, apart from the near ship region. Then the mesh is mirrored, to allow for non-symmetry effects. Then the entire mesh is rotated in such a way that the waves are entering parallel to the length of the domain. Note that the ship is also rotated, effectively resulting in a ship in head waves, just in a different coordinate system than was considered before, see the left picture in Figure 3.6.

To fix this the ship is rotated back to its initial position, without changing the boundaries of the computational domain. The mesh has to adapt in order to allow for this. This is not possible to do in HEXPRESS but it is possible in ReFRESCO. Therefore this step will done using ReFRESCO. In ReFRESCO a deforming grid means that if the ship moves in a certain direction, the mesh deforms to allow for this movement without changing the position of the boundaries of the computational domain, as the wave generation needs to be undisturbed.

In particular, grid deformation based on radial basis functions is used [24]. A radius of deformation is chosen such that it is large enough to not cause numerical errors and small enough that the cells at the boundaries do not need to be deformed. The total number of cells in the mesh resulting from this method is significantly smaller than the number of cells resulting from the previous method, without introducing a significant source of errors. An example of the difference is given in Table 3.3, where the total cell count for a coarse bow quartering mesh is given. Here it is clear that method 1 has a cell count increase of 20 % even for a coarse mesh. For finer meshes this percentage increases significantly. As a result, this method is used throughout this study when creating meshes for quartering waves. The rotation of the ship is depicted in Figure 3.6.

	Method 1	Method 2
Total cell count	2 363 750	1 952 805

Table 3.3: Number of cells in a coarse mesh using the two methods described for the mesh generation.

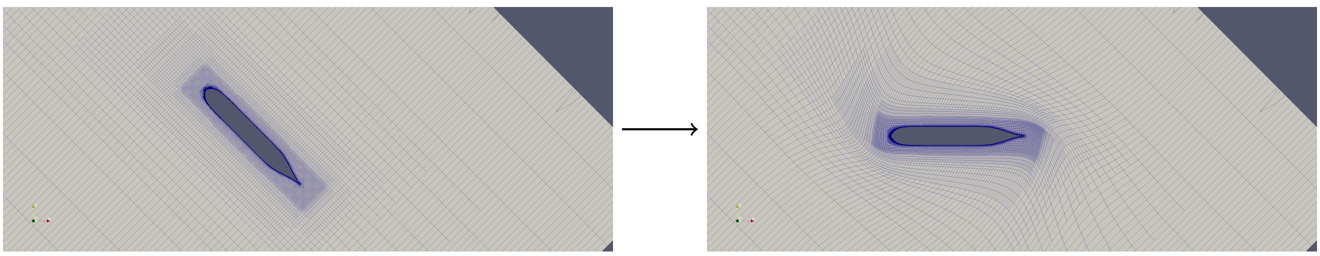

Figure 3.6: *Mesh deformation in response to the rotation of the ship.*

3.1.3 High Frequency Wave Dissipation

Applying the above methodology to the creation of meshes for short quartering waves results in a problem, however. It is found that over half of the wave amplitude is dissipated in such cases. This results in numerical issues, as the wave height is not properly refined for such small waves.

To find out why this is happening, the wave height in the domain during a simulation, of which a snapshot is shown in Figure 3.7a, is investigated. In this figure it is obvious that there is significant wave dissipation present in the complete near-ship area.

The reason for this is a direct result of the meshing strategy. Such a mesh is shown in Figure 3.7b. Here the red line depicts a continuous line of cells. Before the ship was rotated, these cells would be in a straight line perpendicular to the wave direction, see Figure 3.6. Close to the boundaries this is still the case. However, because the ship has rotated, this is no longer the case for cells closer to the ship.

Since it was assumed that the cells in this direction only need to be refined near the ship, the cells quickly increase in size further away from the ship. The mesh deformation resulting from the rotation then leads to large cells that are no longer perpendicular to the wave direction. This is a problem, because now a number of cells are large in a direction in which significant physics needs to be resolved. Because these cells are too large to capture the wave, a part of the solution is lost and the wave dissipation increases.

This problem is resolved by simply adding an extra box in the meshing step. This box is defined by two opposing points given in Table 3.4. The box has a refinement level of 2 in the y-direction. Even such a low amount of refinement makes the cells small enough to properly capture the wave for all cases treated in this report.

	x	y	z
point 1	$-1.5L_{\mathrm{pp}}$	0	$-0.6\lambda + \Delta$
point 2	$2L_{\mathrm{pp}}$	$-L_{\mathrm{pp}}$	$\Delta + A$

Table 3.4: Positioning of the extra box with respect to the stern of the ship.

3.2 Numerical Settings

Then the numerical settings that are used in ReFRESCO are discussed. First the boundary conditions (BC) are given and explained, then the solver settings are discussed. Finally the definition and location of the wave probe is presented.

3.2.1 Boundary conditions

A concise list of the boundary conditions (BC) used in the study are given in Table 3.5. In this section they are treated shortly. The top surface has a pressure BC to ensure continuity with the outside of the domain. In this study deep water is used, meaning that the sea bed is far below the bottom surface of the computational domain. As a result, the BC for the bottom surface is taken to be pressure as well.

The inlet, outlet and side surfaces all share the same wave BC. This BC can both generate and absorb waves, and determines which of the two is needed at a boundary based on the given wave direction and encounter frequency. This makes it an ideal BC for all boundary surfaces that interact with the free surface.

The symmetry BC is only used in head waves and not in quartering waves as the full ship has to be simulated in this case due to the presence of non-symmetrical effects. Finally, the BC at the ship itself is set to slip wall. This BC sets the normal velocity at the wall equal to zero, and the tangential velocity is free. The pressure is set by using a Neumann condition.

3.2.2 Numerical Settings

In this study two types of simulations are done. The first type consist of two separate parts. The first part is a calm water simulation. Here the ship is placed into a domain without waves. At first the ship is not allowed to move, apart from its constant forward speed, to allow the simulation to properly initialize. After a hundred time steps, the ship is allowed to move in the degrees of freedom corresponding to the simulation. The ship will then stabilize at a different position, to account for the effect of the ships movement through the water. During

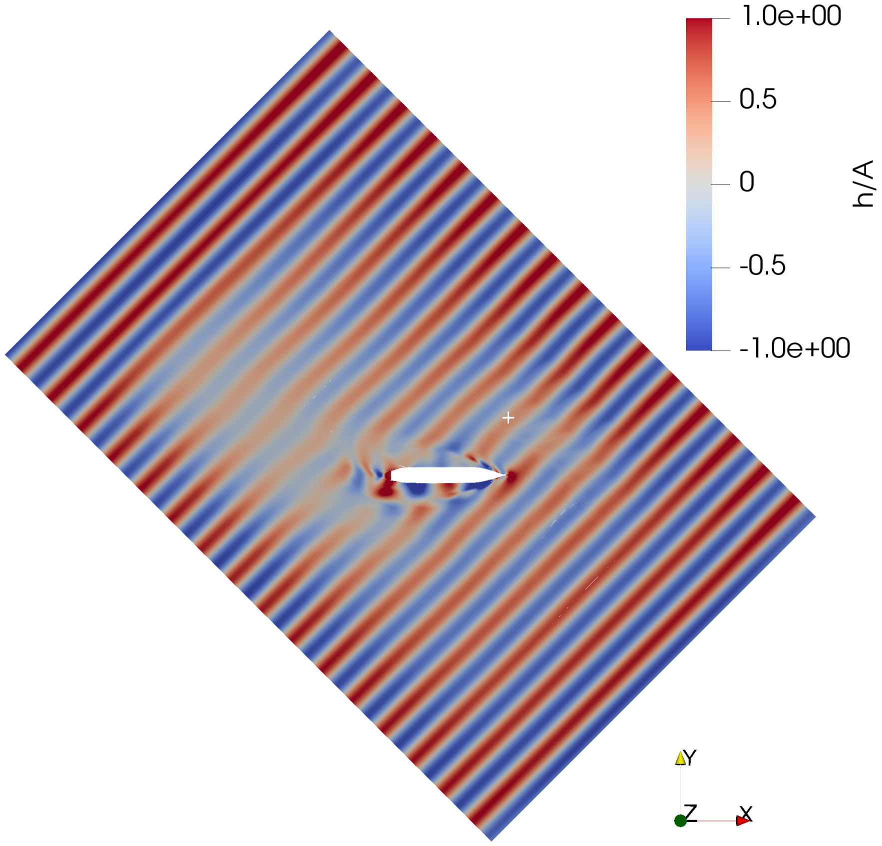

(a)

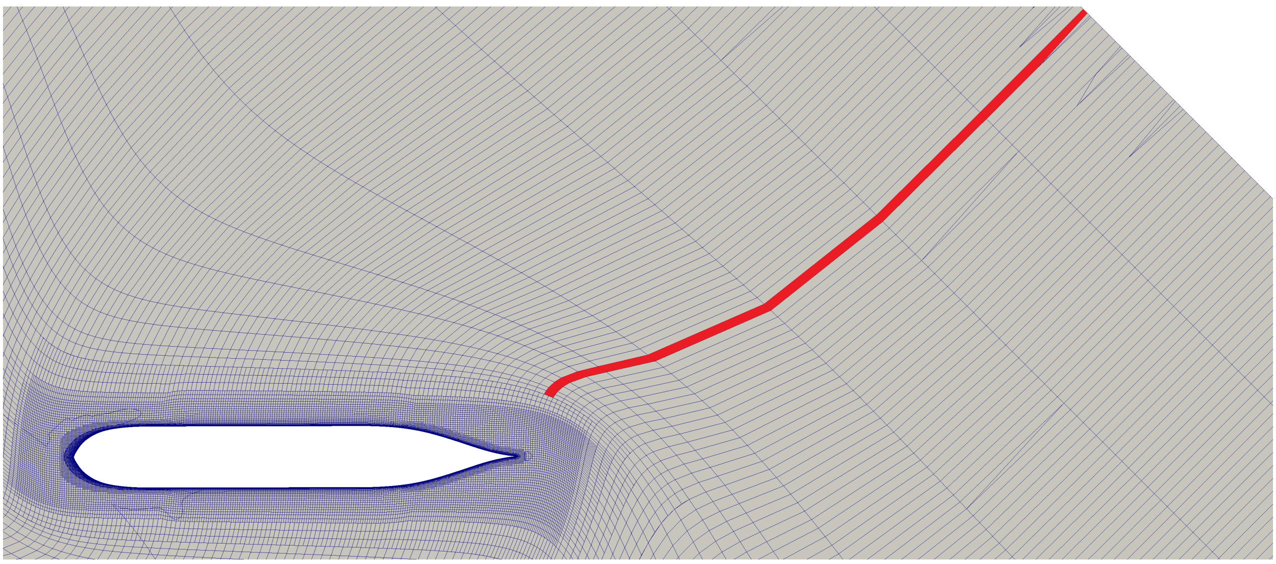

(b)

Figure 3.7: *(a) Contour plot of the wave height normalized by the amplitude. The white "+" indicates the position of the wave probe. (b) Zoom in on the mesh at the draught of the ship. The red line indicates a number of cells that were adjacent before the deformation of the mesh due to rotation of the ship.*

this time a damping zone is present closely around the ship, to ensure that the calm water is actually calm and that there are no numerical errors present that generate wave like structures.

Once a stable calm water solution is achieved, the second part of the simulation starts. Here the waves enter the domain. This is done at the wave boundaries. The exact starting position of the waves is given by

Surface	Boundary Condition
Top	Pressure
Bottom	Pressure
Inlet	Wave
Outlet	Wave
Side	Wave
Symmetry	Symmetry Plane
Ship	Slip Wall

Table 3.5: List of boundary conditions.

the heading. In this study, long waves are defined as waves with a frequency lower than 0.7 Hz, whereas waves with a frequency higher than 0.7 Hz are called short waves. The type of the incident wave, the model that is used to numerically generate the wave, is dependent on the wave frequency. Choosing the wrong wave model could result in instabilities and even crashes of the simulation. In this study long waves are generated using the STOKES5 model, whereas short waves are generated using the STREAMFUNCTION model.

The time discretization is done using the implicit Euler (first order) scheme in the calm water part of the simulation. In the waves part of the simulation the implicit three time level scheme (second order), also known as the backward differentiation formula, is used instead. The time step for the waves is chosen such that there are exactly 200 time steps per wave encounter. The calculation of the residuals is done using the L_2 norm. The tolerance of the time loop is set to 10^{-6}. The settings for the pressure, momentum and free surface equations are presented in Table 3.6.

Parameter	Momentum	Pressure	Free surface
Solver	GMRES	CG	GMRES
Preconditioner	BJacobi	BJacobi	BJacobi
Convergence tolerance	10^{-3}	2.5×10^{-3}	10^{-2}
Max iterations	400	500	200
Minimum implicit relaxation	0.5		0.9
Maximum implicit relaxation	0.9		0.9
Implicit relaxation factor	25		25
Explicit relaxation calm water	0.25	0.2	0.3
Explicit relaxation waves	0.35	0.3	0.35
Convective flux discretization scheme	HARMONIC		REFRICS

Table 3.6: List of numerical settings in ReFRESCO.

The second method that is used in this study is to initialize the the waves over the entire domain at the start of the simulation. This means that it takes less time before being able to get results, as the waves need to fill the entire computational domain in method 1. Using this method, a stable solution is reached quicker. This method is used in systems with a high DoF (4 and over) in bow quartering simulations and in all stern quartering simulations. For stern quartering simulations there is another reason this method is useful, namely to avoid having to wait a large amount of time steps for the waves to cross the entire domain. In the theory it was mentioned that the group velocity of waves in calm water is equal to half the wave velocity. Given this and the velocity of the ship, the waves fill the domain very slowly in stern quartering seas. The numerical settings of a simulation with initialized waves are equal to the wave part of the simulation of the first method.

3.2.3 Preparing the results

For the calculation of RAO and QTF it is important to have a good estimate of the wave height as the wave reaches the ship. The wave amplitude is an input parameter to the simulation, but this value only holds in the absorption region near the boundaries. As the wave is travelling towards the ship, it loses energy due to diffusion, both numerical and physical, and as such the wave height decreases. Thus, the amplitude of the wave needs to be measured during the simulation. This is especially important for coarse grids, as the wave amplitude deprecation is higher in this case.

Determining the wave height is done using a wave probe. The wave probe is located at a chosen position and simply measures at which position along the z-axis the air volume fraction is equal to 0.5 at every time step. For a wave probe that is undisturbed by the ship and located close to it, the wave height at the wave probe can be taken to be equal to the wave height at the ship. Undisturbed by the ship means that it is not too close to the ship, not in a wedge behind the ship and not located such that the waves have already passed the ship before reaching the wave probe. The chosen position of the wave probe used for calculations is sketched in Figure 3.8, together with the domain, the ship and the absorption zone.

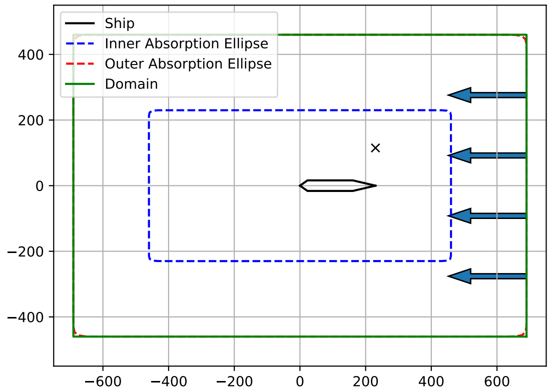

(a) *Bow Waves*

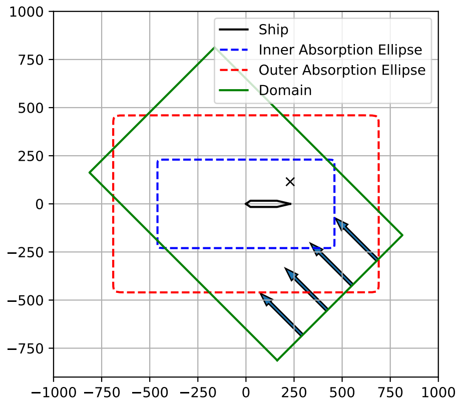

(b) *Bow Quartering Waves*

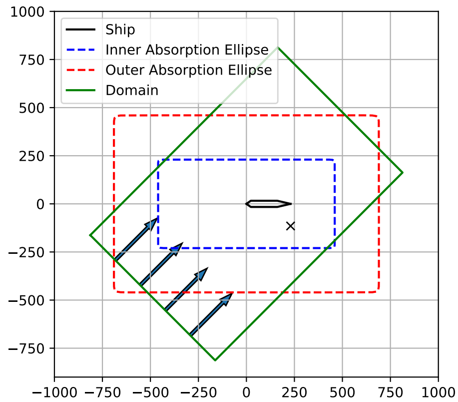

(c) *Stern Quartering Waves*

Figure 3.8: *Sketch of the position of the wave probes with respect to the ship, the domain and the absorption zone. The arrows give the direction of the incoming waves.*

3.3 Gathering of Results

In this section all the different cases investigated in this thesis are explained in detail, starting with head waves only considering pitch and heave, leading up to stern quartering waves considering all 6DoFs. A number of models that are used in these cases are also explained.

3.3.1 Spring Models

Heave, roll and pitch all have a physical equilibrium position. For the other three DoFs (surge, sway and yaw) however, there is no stable position for the ship to move to. However, the ship should not rotate too much around the z-axis, nor should it move away from the centre of the computational domain too much. The reason for this is numerical; if the ship overly strays from the initial position, then the mesh needs to be overly deformed which will result in numerical errors. For yaw there is also a physical reason why it cannot stray from the stable position too much, as the response of the ship is dependent on the heading. A difference in yaw from the initial position effectively also corresponds to a difference in the heading. For yaw values of a few tenths of degrees this is not a problem, since the change in the response of the ship due to the heading is generally low, but for higher yaw deviations this could significantly impact the results. Moreover, the velocity with which these deviations occur could influence the force response of the ship and should thus be minimized.

Therefore a method has to be devised that artificially creates a stable position for the ship in surge, sway and yaw in such a way that it does not significantly impact the ship response and that the ship does not move from the initial position too much. In this report a few such models are used, all based on springs. These models are discussed in this subsection.

Initial spring model

In this method an external conceptual force, i.e., one with no physical basis, is added to the system that acts on the ship in such a way that this force pushes the ship back to its initial position. This force is not a constant, but is dependent on the deviation. Much like a spring, this force is zero when the ship is in its initial position, and the further it deviates, the higher this force becomes. Due to the similarities between this force and a spring, it is straightforward to use the spring equation, or Hooke's law, to calculate it. Hooke's law is given in Equation 3.1.

$$F = kx. \tag{3.1}$$

Here F is the added force, x is the deviation from the initial position and k is the stiffness constant. The stiffness constant for a certain case can be calculated by using the mean force on the ship for that DoF in a previous case, or can be taken from the FATIMA results.

The reference length for sway and surge is taken to be half the breadth of the ship. The reference rotation is taken to be 0.2 degrees. These reference values are chosen such that they allow the ship to deviate enough to get a reasonable solution, without becoming so large that the deformation of the grid, due to the movement of the ship, becomes too much for ReFRESCO to handle, as that would result in the simulation crashing.

Single and double RAO spring model

The next model that is used in this study is similar to the initial spring model. Once more a spring is used to push the ship towards the initial position. However, to keep the mesh deformation as low as possible, a new method for defining the stiffness constants of the springs is devised. In this method the stiffness constant is calculated using both the QTF as well as the RAO for the respective motion. These values are of course not known in advance but can easily be approximated by using the corresponding FATIMA solution.

In particular, instead of using the rather arbitrary values of 16.1 m and 0.2 deg for x_0, the motion amplitude is used. The reference length is equal to the RAO of the corresponding motion times the corresponding wave amplitude. This results in the equation for the stiffness constant given in Equation 3.2. Using this method a mean deviation from the initial position that is equal to $RAO \times A$ is theoretically achieved.

$$k = \frac{F}{x_0} = \frac{QTF \times A^2}{RAO \times A} = \frac{QTF \times A}{RAO} \tag{3.2}$$

This model is called the single RAO spring model. The downside of this model is that it is possible that the spring is so stiff that it might have a non-insignificant effect on the motion response of the ship, since it is calculated to precisely allow for the motion necessary for the RAO but nothing more. To minimize this effect, a safety factor of 2 is build into the model by multiplying RAO by 2 in 3.2. The model is then referred to as the double RAO model.

Finally, to achieve a mean deviation of 0, an extra force can be added to 3.2 equal to $-QTF \times A^2$. This extra constant force essentially adds a pretension to the spring, and is used to ensure that the ship oscillates nicely around the initial position.

Rudder

The final method that is used in this study is that of a computational rudder model. Here the PD model is used [25], which is essentially the same method as the springs, where an external force is added to the equations of motion at every outer step in the simulation. However, the spring model only considered the zeroth order influence of motion, i.e displacement. The PD model also considers the first order influence, i.e. velocity. The result is equivalent to a dampened spring, for which the equation is given in Equation 3.3. Here x is the yaw motion in rad, D is the damping, P is the spring constant and F is the added moment.

$$F = D\frac{\partial x}{\partial t} + Px. \tag{3.3}$$

To ensure that the stable position of the ship is the same as the initial position, the rudder is positioned in the same direction as the ship, meaning that it always adds a moment that pushes the ship back to the initial position. The calculation for the damping and stiffness constant of the rudder is given below, and is based on lifting surface theory [16].

In lifting surface theory it is possible, for a known rudder geometry, to calculate the corresponding drag and lift constant. From the ship speed, equal to 16 knots in this study, the calm water resistance has been experimentally determined to be 1250 kN [26]. This is used to calculate the thrust of the propellers, using Equation 3.4. Here t is the thrust deduction factor, approximated to be 0.15. n is the number of propellers for the KCS and is equal to 5. From the thrust the propeller outflow velocity can be determined. Finally, it is known that the propeller outflow velocity is proportional to the rudder inflow velocity, since the rudder is located right behind the propeller. This allows for the calculation of the drag and lift forces of the rudder, given in Equation 3.5 and 3.6, respectively.

$$Th = nR/(1-t) \tag{3.4}$$

$$F_{\mathrm{L}} = \frac{1}{2}\rho v_{\mathrm{in}}^2 AC_{\mathrm{L}} \tag{3.5}$$

$$F_{\mathrm{D}} = -\frac{1}{2}\rho v_{\mathrm{in}}^2 AC_{\mathrm{D}} \tag{3.6}$$

Since the distance from the rudder to the CoG of the ship is known, this allows for the calculation of the moment of the rudder. Here the damping coefficient and spring constant of the rudder, equal to 3 rad/deg and 9.23 rad s/deg for the KCS, respectively, are used to determine the rudder angle. The resulting moment is normalized by the amplitude of the resulting yaw angle, calculated from the RAO, and the encounter frequency. The moment calculated using the damping coefficient of the rudder then gives D, while the moment calculated using the spring constant of the rudder gives P.

3.3.2 Head Waves

The first and most simple case that is considered is a ship in head waves. Since there are no 3D effects, only a half-ship needs to be simulated, with a symmetry plane running along the length of the ship through the middle. Only two degrees of freedom are considered in this situation: heave and pitch. While this case is not very interesting in and of its own, it does allow for a simple check on whether the methods and numerical choices made in the CFD are realistic, and how they compare to experimental results. This gives a possibility to find any issues with the CFD in the most basic use case, before moving on to more complex problems.

3.3.3 Bow Quartering

The next case is a ship in bow quartering waves. Now the system is no longer symmetric, which means that 3D effects will play a significant role. First this problem is done in 2DoF, once more using heave and pitch. Thereafter, a third DoF is added on top of these, roll. Roll is chosen as the third DoF because it has a physical equilibrium position.

Once roll is investigated the system is expanded to include a fourth DoF. Both sway and yaw are separately considered in a 4DoF system in order to get the workings of such a system correct. There is no need to investigate surge separately, as surge and sway are very similar. To be able to set the fourth DoF free, a spring model as defined in the previous subsection is used.

Once the 4DoF system is working reasonably well, a 5DoF system is considered. Sway and yaw are now taken into account simultaneously. The same spring models that were used in the 4DoF systems are now used simultaneously, as they work independently of each other. Once this works reasonably well, a new spring for surge is also added and the full 6DoF system is considered.

3.3.4 Stern Quartering

Finally a ship in stern quartering seas is considered. Here the full 6DoF system is investigated immediately. Any method that was used in the bow quartering seas cases, in particular with relation to the spring model, is immediately used in stern quartering. Roll damping is added here as well, since the roll is expected to be significantly higher for this case compared to the bow quartering, making this an important addition to the model.

3.3.5 Overview of cases

Once a 6DoF methodology has been found, it is applied to a number of different cases with different amplitudes and frequencies as to investigate the influence of these parameters on the found methodology. These cases are designed to give a good feel on the influence of amplitude and frequency variation in the least amount of simulations and are presented in Table 3.7. It should be noted that all configurations are chosen such that corresponding experimental data is available. Moreover, it can be seen that $\tau > 0.25$ in all cases.

	ω	A	ω_e	τ
Head Waves	0.525	0.75	0.756	0.635
Bow Quartering Waves	0.5	0.75	0.648	0.544
	0.575	0.75, 1.00, 1.25, 1.50	0.771	0.647
	0.625	0.75	0.857	0.719
	0.75	0.75	1.084	0.909
	0.85	0.75	1.279	1.073
Stern Quartering Waves	0.55	0.75	0.371	0.311
	0.675	0.75, 1.00, 1.25	0.405	0.340
	0.75	0.75	0.416	0.349
	0.85	0.75	0.421	0.354

Table 3.7: Overview of the parameter settings of the cases to be run in a 6DoF system.

3.4 Analyzing Results/Postprocessing

In this section some important aspects of postprocessing are explained. These aspects are in particular related to RAO and QTF calculation and the validation of the CFD software.

3.4.1 Deriving RAO and QTF

The results of the simulations are presented in terms of RAO and QTF of the 6 DoFs. The motion of the ship in the experimental work is measured at the CoG, where a measurement system is placed that calculates the motion of the ship in terms of the 6 DoFs. In the simulations this is done analogously, to ensure that a valid comparison between the numerical and experimental work can be done. Here the motion of the ship is calculated by determining the displacement of the CoG with respect to its initial position.

The RAO and QTF are calculated using a harmonic analysis. In this analysis a harmonic function of second order is fitted to the data. This is done using the last 8 waves encountered in the simulation, unless specified otherwise. The amplitude of the first order of the harmonic function then corresponds to the amplitude of the corresponding wave response. This analysis is done on both the ship response as well as on the wave probe result.

It should also be noted that the RAO corresponding to all translations and rotations are of interest in this study, because all motions oscillate due to the wave, but not all corresponding QTF. The reason for this is the physically stable positions for heave, roll and pitch as was explained in the Spring Models section. A physically stable position results in a mean displacement of the ship in these DoFs equal to zero. Since there is no external force added in the corresponding directions, this means that the mean added wave force on the ship also has to be zero in this direction. This means that the corresponding value for QTF is zero.

3.4.2 Validation

All results are compared to both results generated using FATIMA and, where possible, to experimental results. FATIMA is a time and frequency domain Rankine potential flow solver. It uses steady flow results from a non-linear potential flow code called RAPID, also developed at MARIN, as a basis for the linearization of the unsteady boundary conditions at the free surface and at the ship hull [27]. For the motion response of the ship FATIMA gives a reasonably accurate result. For the force response of sway and yaw the FATIMA results should be considered an upper bound. For these parameters no experimental results exist.

Moreover, FATIMA does not take into account the amplitude of the waves. In FATIMA the RAO and QTF calculation is done using waves of infinitesimally small amplitude. When comparing this to CFD and experiments, an underlying assumption has to be that the RAO and QTF are independent of the wave amplitude. Once a working 6 DoF system is established, the dependency of RAO and QTF on the wave amplitude is further investigated using the CFD model.

Finally, experiments are not perfect. One particular issue is the difficulty in controlling the wave frequency in a basin. As a result, it is possible that the actual frequency during the experiments was slightly different than the reported frequency. If the derivative of a particular RAO with respect to the frequency is small, this discrepancy will not significantly affect the results. However, in cases where the derivative is large it is possible that there is a significant error in the experimental results.

4 Results and Discussion

In this chapter the results from the simulations are discussed, together with the corresponding analysis. Since the goal of this study is to find a methodology for fast and robust calculation for a ship in quartering waves, a relatively coarse grid will be employed for this purpose. This allows us to study and solve any potential issues that come up, without being limited by the computational time it takes to test solutions. Once a methodology has been developed a grid convergence study is done to study the influence of the grid on the results.

The methodology presented here is developed using a case with a specific wave frequency and wave amplitude. In particular, for head waves $f = 0.525$ rad/s and for bow quartering waves $f = 0.575$ rad/s is used. $A = 0.75$ m is used for both cases. These cases are chosen such that multiple experimental data points are available for comparison. After the methodology has been developed, the effect of wave amplitude and frequency on the motion and force response of the ship is investigated. This is done by applying the found methodology to a range of cases with varying amplitude and frequency in both bow and stern quartering seas.

4.1 Head waves

The first case that is investigated is the KCS in head waves. This is a very simple case, and is therefore a good starting point. This simulation is done by first running a calm water simulation, followed by a simulation where the waves are gradually filling up the domain.

The results from this simulation in terms of heave and pitch motion as a function of simulation time is given in Figure 4.1. Here a few numerical choices have been made that are reflected in these time traces. The first is that during the first roughly 50 seconds, no motion of the ship is present for heave and pitch. This is because the motion in all DoFs is restricted during this time. Due to the initialization, there exist some large non-physical forces in the fluid that could have a large effect on the ship at the start of the simulation. After some time these have dissipated, at which point the motions can be set free.

Once the motions are set free, the ship relaxes to the stable position during the next roughly 100 seconds. Then the calm water simulation is continued for another 400 seconds. This is to ensure that the ship is fully stable. Since the time step during this period is large, relative to the time step during the simulation with waves, simulating calm water for such a large amount of time is not computationally expensive. Once the waves come into the domain, the time step is decreased such that 200 time steps coincide with a single wave period. An unintended by-product of this variation in time steps is that the result of the wave part of the simulation is hard to see in figures like Figure 4.1, since the calm water part of the simulation is ran for a longer simulation time and thus takes up nearly the whole figure.

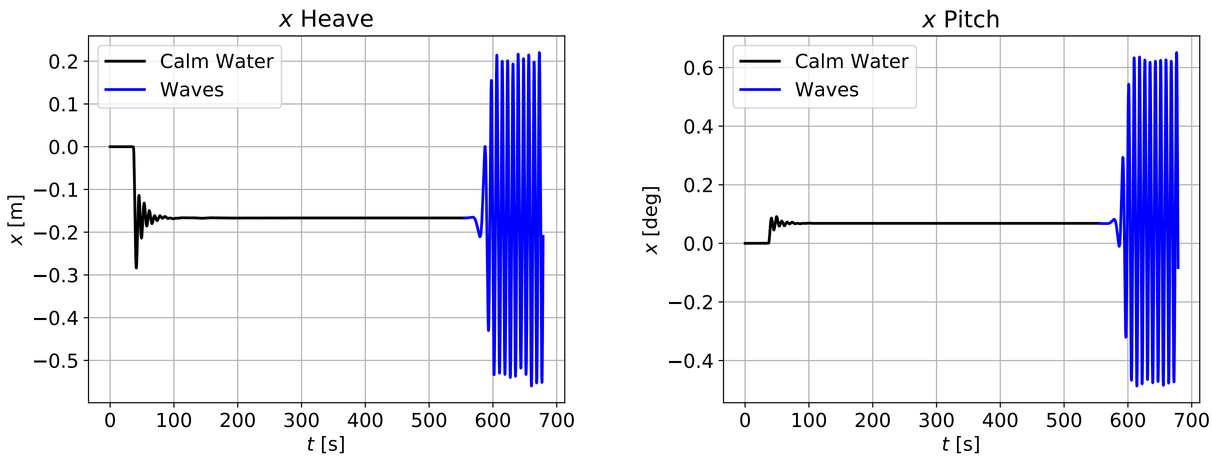

(a) (b)

Figure 4.1: *Time traces of the displacement in heave (a) and pitch (b) for a ship in head waves.*

To alleviate this issue the figures are presented in a different manner. The calm water part of the simulation is not shown as it simply shows the ship relax to a new stable position. Instead only the wave part is shown, which allows one to see clearly what happens to the ship motions during a single wave period. In this case the motions are also shown as a function of time steps, rather than simulation time. This is done here to show that one oscillation is indeed equal to a single wave period, as every oscillation takes place over 200 time steps.

This approach results in Figure 4.2. Here the response of the ship to the waves can be clearly seen. Before the waves arrive at the ship, the ship is in a constant stable position. The first few waves are not yet of the proper wave height, due to the decay of waves at the front of the group, and can be seen as the wave initialization period. For the last roughly 1000 time steps though, there is a clear oscillatory motion. It is clear that this motion is not perfectly stable, as there exists some numerical noise.

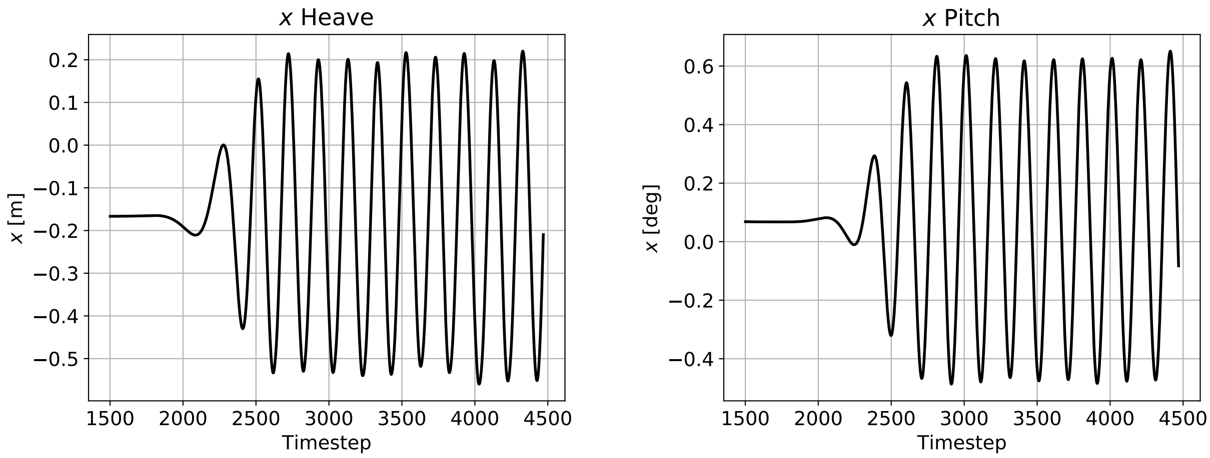

(a) (b)

Figure 4.2: *Time traces of the displacement in heave (a) and pitch (b) during only the wave part of the simulation for a ship in head waves.*

To combat the influence of this noise on the results in terms of RAO and QTF, the results are averaged over a number of wave periods, as mentioned in the Method chapter. In this case only the last 4 wave periods are used. The resulting RAO and QTF are shown in Figures 4.3 and 4.4 respectively.

From these figures it is clear that all three solution sets, generated with FATIMA, experiments and CFD, are in reasonable agreement about the resulting values. There are a few reasons why this agreement is not perfect though, that also impact the rest of the CFD results presented in this thesis. The first is that the CFD is done on a rather coarse grid. This means that it is possible that the result for a finer mesh is closer to the experimental results. The exact influence the mesh has is studied in a grid convergence section, after a working methodology for the 6DoF systems has been devised.

A second reason is that both the FATIMA calculations and the experiments are not executed using only 2 DoFs, unlike the CFD, but rather in a 6DoF system. It is thus assumed that the translational and rotational motion along the different axes are independent of one another. This is true to an extent, enough for the results to be of the same magnitude. However, there is an error introduced by doing this. The magnitude of this error varies for the different DoFs.

Taking these possible error sources into account, as well as those mentioned in the Validation section of the Method chapter, the results presented in the aforementioned figures can be concluded to show reasonable agreement. Thus it can be determined that the CFD code fairly accurately determines QTF of surge and RAO of pitch and heave in head waves.

4.2 Bow quartering waves

Then bow quartering waves are considered. It should be noted that the time traces, RAO and QTF values are not all given here for every simulation. Instead, only the results which are of interest for that particular case are shown. The behaviour of the results that are not shown can be assumed to be in line with the previous simulations.

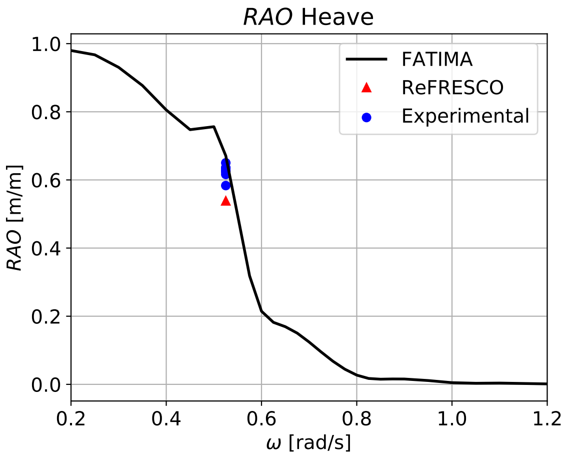

(a)

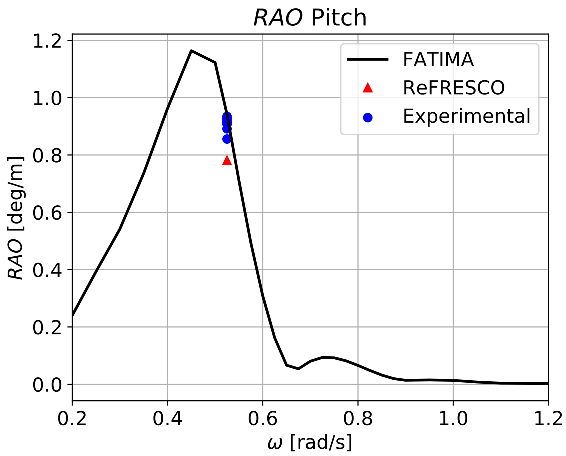

(b)

Figure 4.3: *RAO of Heave (a) and Pitch (b) as a function of frequency for a ship in head waves.*

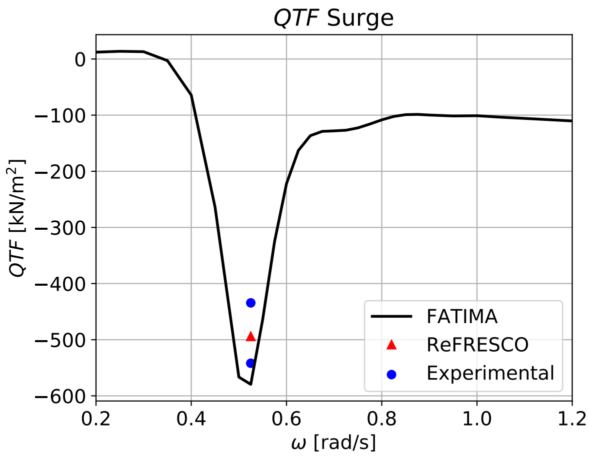

Figure 4.4: *QTF of surge as a function of frequency for a ship in head waves.*

4.2.1 2DoF (heave and pitch) and 3DoF (heave, roll and pitch)

In order to ensure that the change in wave direction does not induce any new errors, the first simulation in bow quartering waves once more only considers heave and pitch. Looking forward to the other DoFs that will be added to the system, it is a good idea to take a look at some of the forces acting on the ship, specifically the forces for which QTF is of interest. These are plotted in Figure 4.5. In this time trace and those following, the dashed line gives the moving average over a single wave period of the corresponding graph. Here it is expected that at the start of the simulation, before the waves enter the domain and after the ship has stabilized, $F_y = M_z = 0$. The reason for this is that the problem is symmetric before the waves arrive at the ship. However, this is not what is shown in the figure, as a clear non-zero value is seen for all forces.

These forces are non-physical, and are a result of the mesh. For simulations with more than 2DoF this force will be cancelled in the simulation by adding equal and opposite forces as constant external forces to the equations of motion. The value of these forces are taken from the result of the 2DoF calm water simulation. The value of these non-physical forces is mesh dependent. The same methodology is also applied to the roll moment, as even though the corresponding QTF is not of interest, the roll force has to be 0 due to symmetry.

For F_x a constant force is expected, resulting from the ship moving through calm water. However, the ship should move at a constant speed and should not move out of the computational domain, even when surge is eventually set free. To ensure this, the force in the surge direction due to calm water is also cancelled by an external force. This prohibits the ship from moving away under influence of the calm water once surge is set free. Doing this ensures that the forces found in the simulations are equal to the wave added resistance in their respective direction.

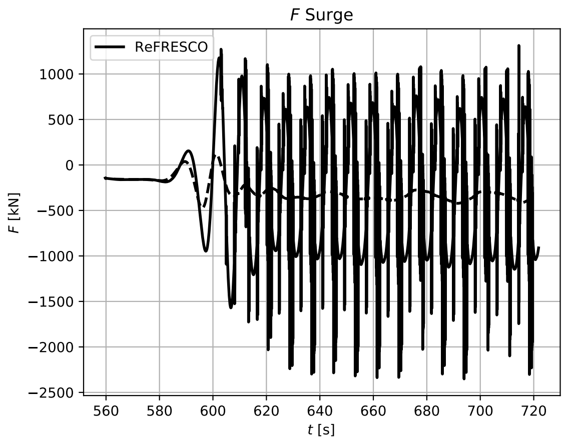

(a)

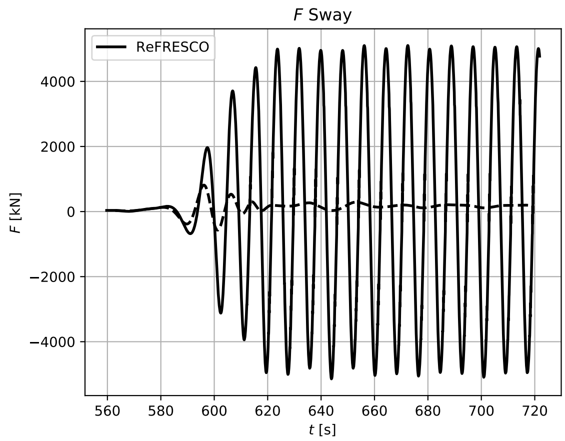

(b)

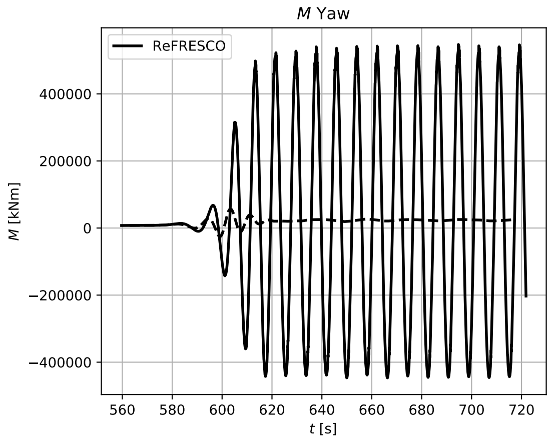

(c)

Figure 4.5: *Time traces of the force in surge (a), sway (b) and the moment in yaw (c) in a 2DoF system.*

The result of both the 2DoF and the 3DoF simulations in terms of the motion and force response is shown in Figure 4.6 and 4.7, respectively. It can be seen here that no new issues arise when changing from a ship in head waves to a ship in bow quartering waves, as the results from the CFD match reasonably well with the experimental and FATIMA results for heave and pitch, similar to the head waves case.

In the 3DoF simulation it can be seen in the *RAO* result for roll, Figure 4.6c, that the experimental results are significantly more divided than was the case for heave and pitch. Moreover the Fatima result is even lower than the minimum of these values. This could point to a larger inaccuracy in the results for roll, which is good to keep in mind for future comparisons. This behaviour is also seen in the time trace of roll, Figure 4.6d, for which it is clear that noise has a relatively large effect on the roll behaviour of the ship. This is filtered out of the *RAO* result by averaging over a number of wave periods and by doing the calculation with respect to a moving average, but it does indicate that roll is more sensitive to changes than heave and pitch.

4.2.2 4DoF (sway, heave, pitch and roll)

Then a fourth DoF is added to the system. It should be noted that from now on the waves are initialized over the entire computational domain at the start of the simulation. As a result the time step is kept constant during the entire simulation time. The resulting sway motion in this case is given in Figure 4.8. Here it is clear

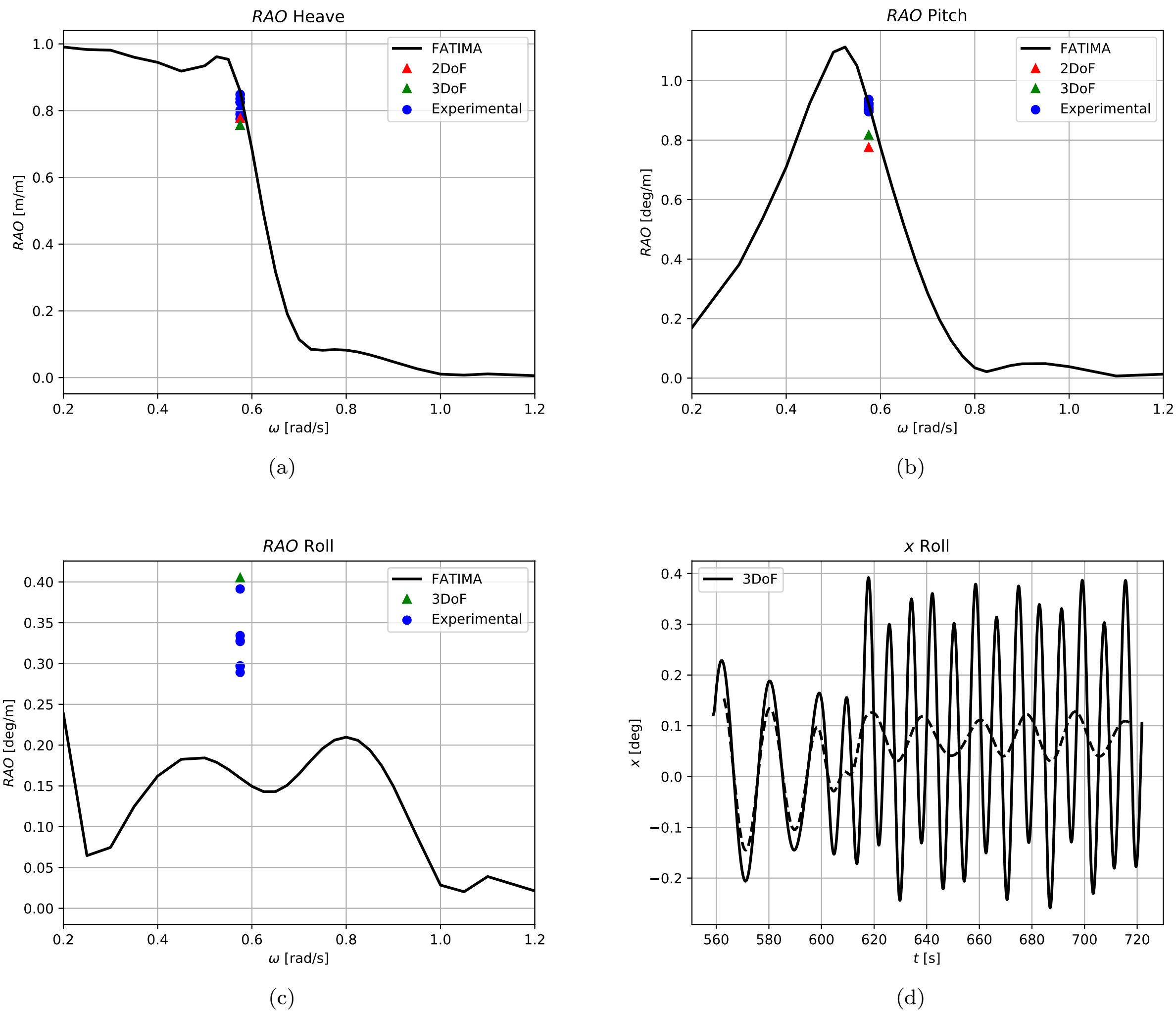

(a) (b) (c) (d)

Figure 4.6: *RAO of heave (a), pitch (b) and roll (c) as a function of frequency and the time trace of roll (d) for a sailing ship with 2DoF and 3DoF.*

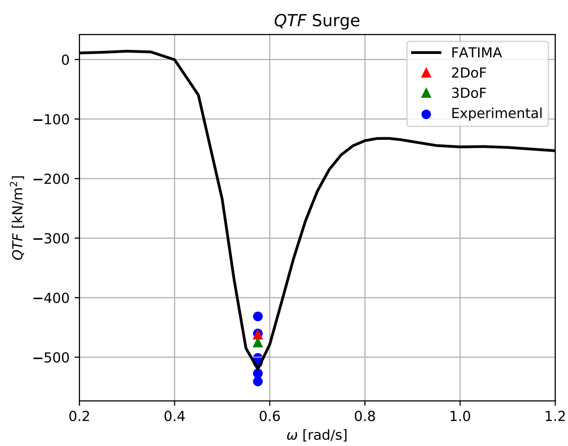

Figure 4.7: *QTF of surge as a function of frequency for a sailing ship with 2DoF and 3DoF.*

that every wave pushes the ship further away from the initial position. This phenomenon is called drift and is present only when there is no equilibrium state for a motion.

The issue with drift is that the force in the corresponding direction is affected by this phenomenon. This is a problem because drift was not present in the simulations done in FATIMA, making it impossible to compare it to the CFD. For the motion response drift is not an issue, since the oscillations are evaluated with respect to a moving mean. To solve the problems in the force response, a different method needs to be devised, in which the ship is allowed to move under influence of a wave, but does not move significantly over a full wave period.

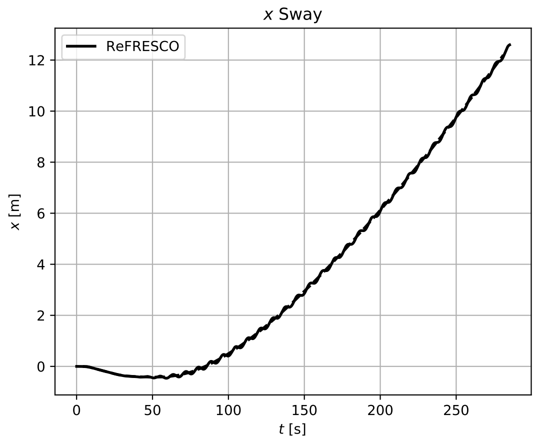

Figure 4.8: *Time trace of the displacement in sway for a sailing ship with 4DoF without using a spring model to counter sway drift.*

Added spring force

In order to solve the issue with drift, the initial spring model is used with the spring constant calculated from the force response in the 3DoF simulation. Ideally, the ship will oscillate around the chosen x_0 value. This is the case when the mean force does not change due to the corresponding motion being set free. In practice this is of course not the case, as the presence of another DoF changes the force response. However, the forces will be in the same order of magnitude, giving a reasonable value for the stiffness constant that allows the ship to deviate enough to get a reasonable solution, without becoming so large that the movement deforms the grid too much.

Another problem is also present, namely that the ship needs a lot of time to reach the stable solution. In Figure 4.8 it was shown that the ship only translates by 12 m after 7000 time steps. This is already a significant computational cost, and waiting for the ship to reach 16.1 m costs even more. To solve this problem, the ship is translated by x_0 at the start of the simulation. This significantly decreases the time needed for the ship to reach the stable position.

The result of using such a spring force is shown in Figure 4.9. Here a significant improvement over the motion depicted in Figure 4.8 is shown, evidenced by the clear decrease in drift. However, the result can clearly still be improved upon. It also turns out that the spring introduces a large-scale oscillation in the system, which can be seen by the sway decreasing at the start of the simulation, but increasing at the end.

The reason for this is that the spring force is used in the equation of motion calculation from the start of the simulation, even though the waves are dampened by a damping zone around the ship at the start of the simulation. The damping zone ensures the simulation initializes without issue. This means that the spring force is dominant in this part of the simulation, which drives the ship to move towards the origin. Once the damping zone is turned off and the waves start to effect the ship, the ship is already significantly displaced from the x_0 position. As a result the spring force does not fully cancel the drift effect. Furthermore the ship drifts beyond the stable position, as the ship has a non-zero velocity when it reaches it. Over time this effect will dampen out and the ship will reach a stable oscillatory motion. However, waiting for this effect to dampen out takes too much computational time, and is thus not a viable solution to this problem.

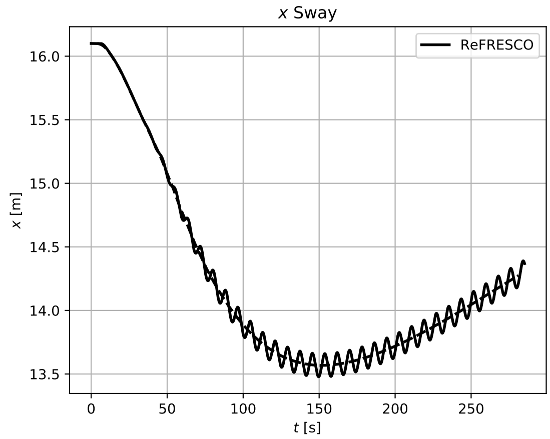

Figure 4.9: *Time trace of the displacement in sway for a sailing ship with 4DoF using the initial spring model to counter sway drift.*

Proposed solutions

To cancel the effect of the large scale oscillation introduced by the spring, three different methods have been devised. These methods are introduced in this section with respect to sway, though they can be used analogously for surge and yaw.

Method 1 is similar to the simulation referenced in the previous subsection, where a spring force and an initial translation are used. The difference in this method is that all motions are fixed until after the damping zone is turned off. This is done by setting the under-relaxation of the ship free motion to 0. Once the wave effect is properly initialized, all motions are set free simultaneously by gradually increasing the under-relaxation from 0 to 1 over the duration of three wave periods.

Method 2 sets all motions free at the beginning of the simulation, similarly to the initial case. To ensure that no drift takes place while the wave damping zone is present, the spring force is turned off at the start. Moreover, another external force is added that is equal and opposite to the hydrodynamic force in the sway direction. This means that, ideally, there is a net force of zero on the ship in the sway direction and thus no motion. Effectively the sway motion is thus turned off for the start of the simulation, while heave, roll and pitch are free. Once the wave damping zone has been turned off completely, the external force is linearly changed from the hydrodynamic force to the spring force over three wave periods.

Method 3 is a combination of method 1 and method 2. At the start of the simulation, method 1 is employed to fix all motions for a large amount of time steps. Then, once the waves are initialized fully, the under-relaxation of the motions is gradually increased from 0 to 1 over the duration of a single wave period. However, an external force equal and opposite to the hydrodynamic force is applied in the sway direction during this time. Once the under-relaxation is equal to 1, the hydrodynamic force is linearly changed to the spring force over the duration of 3 wave periods, similarly to method 2.

Results

In this subsection the results from the simulations using the three aforementioned methods are compared in terms of motions and forces. The simulations are created in such a way that the only difference between them is the method that is used for the wave effect initialization. The wave definition, mesh and stiffness constant are the same between the different simulations and are the same as were used for the two previously mentioned simulations.

In Figure 4.10 the sway displacement resulting from these three proposed methods is compared to the two simulations without initialization methods. Here it is clear that the drift issue is largely solved using any of the three proposed methods. While there is still some drift present in the simulation, it is insignificant and is not expected to impact the force response of the ship.

Time traces of the sway motion using the three proposed methods are depicted in Figure 4.11. Here it turns out that the choice of the initialization method does have impact on the sway motion. For method 2 it can be seen that the cancellation of the hydrodynamic force does not work perfectly. This is because of numerical noise

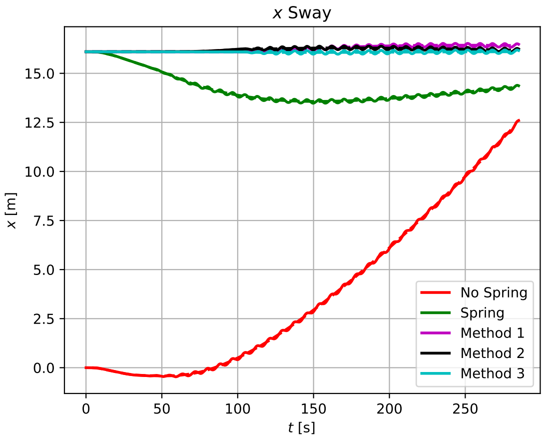

Figure 4.10: *Time trace of the displacement in sway for a sailing ship with 4DoF using the three proposed initialization methods compared to the simulation using no spring, and using the initial spring model for sway drift.*

in the simulation, making it difficult to perfectly mimic a counter force at every outer step of the simulation. As a result an increasing displacement over time is present, which goes to zero when the effect of the waves and the spring force is taken into account. While this does not cause an issue in this particular case, it might cause issues when applying this to other cases, such as in stern quartering seas or yaw motion simulations.

Method 1 also has a displacement at the initialization, the amplitude of which is slightly larger than using method 2. However, in this case the displacement is a result of physics, rather than noise. The other motions, heave, pitch and roll, are being turned on at the same time as sway, whereas in the other two methods these are already stabilized when sway is first taken into consideration. The interactions between these motions cause some sway effects at the start-up, which result in a displacement. Because there is a physical reasoning behind it, the amplitude of the displacement is not foreseen to become a problem when simulating more difficult cases.

Method 3 does not have these kind of issues. The drawback here is mostly in its complexity. Because it is a combination of the other two methods it is significantly more complex than either separate method, and requires more complex user code to run. This means that if another, simpler, method can get the same results, despite the aforementioned issues, it is better to use that method instead.

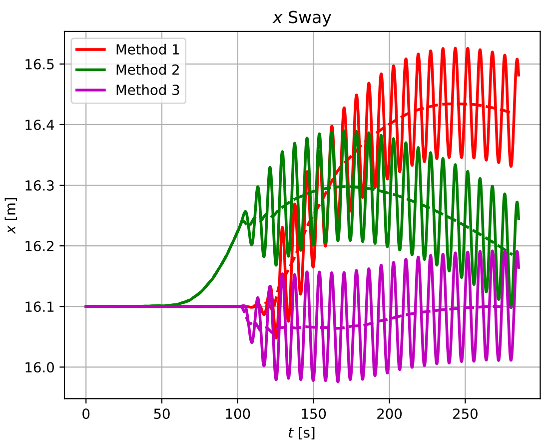

Figure 4.11: *Comparison of time traces of the displacement in sway in a 4DoF system making use of the 3 different spring model initialization methods for sway motion.*

The corresponding *RAO* values are shown in Figure 4.12. Here it is clear that there is no significant influence of the methods on the *RAO*. All three methods show good comparisons to both experimental results and to

FATIMA in all DoFs and there are only insignificant differences between them.

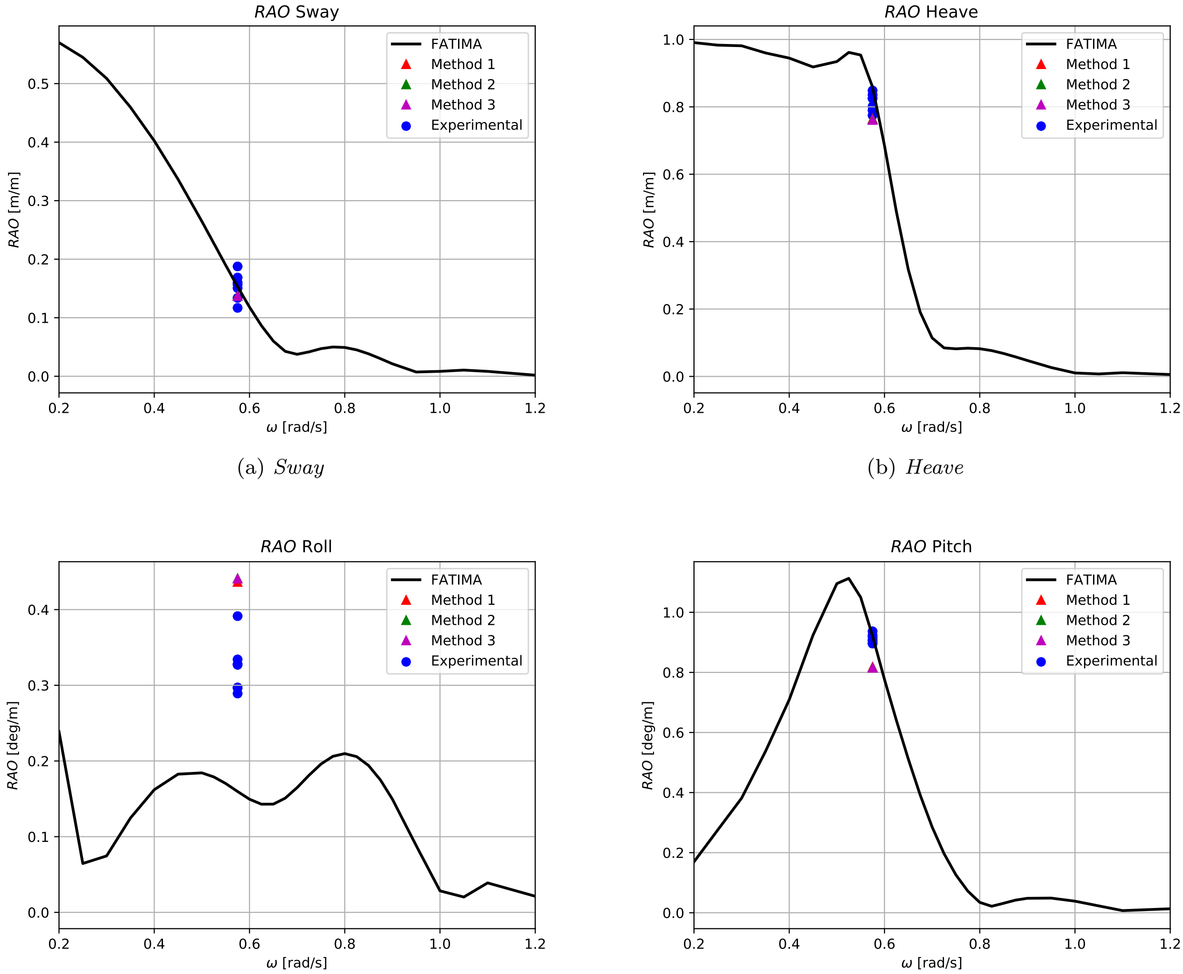

(a) *Sway* (b) *Heave*

(c) *Roll* (d) *Pitch*

Figure 4.12: *RAO of sway (a), heave (b), roll (c) and pitch (d) as a function of frequency for a sailing ship with 4DoF.*

Based on the motions above it was concluded that the amplitude of the sway drift was not significant enough to impact the forces in any of the proposed methods, but it is significant enough in the two initial cases. This can also be seen from the behaviour of QTF in sway, plotted in Figure 4.13. Here it is clear that the proposed methods all result in practically the same value for the sway QTF, whereas the value given by the simulation without a spring is considerably different, and the simulation with spring force is in between. From this a provisional conclusion on the effect of the drift can be made, namely that a larger drift amplitude results in a lower value of the corresponding QTF.

The result of the proposed methods in terms of time traces of surge and sway is given in Figure 4.14. The main point in this figure is that all methods reach the same stable oscillation in a relatively short amount of time steps. In particular, this state is achieved after less than 150 seconds, corresponding to roughly 4000 time steps, for both the surge and sway force. The instantaneous values of the forces and the moving force average are also overlapping, indicating that the choice of initialization method does not significantly impact the response of the ship to waves in terms of the forces.

The resulting QTF values are plotted in Figure 4.15. For both QTF values and all three methods, this comparison is reasonable. It is clear that there is no significant difference in the force response of the ship when using any of the three methods. As a result, all three methods are said to work reasonably well. Therefore method 1 is chosen to be used in all upcoming sections, because it is simpler than the other methods.

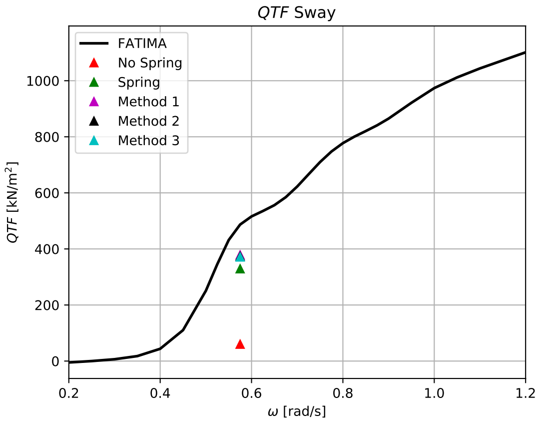

Figure 4.13: *QTF of sway (a) as a function of frequency for the three proposed methods compared to the two previous simulations for a sailing ship with 4DoF.*

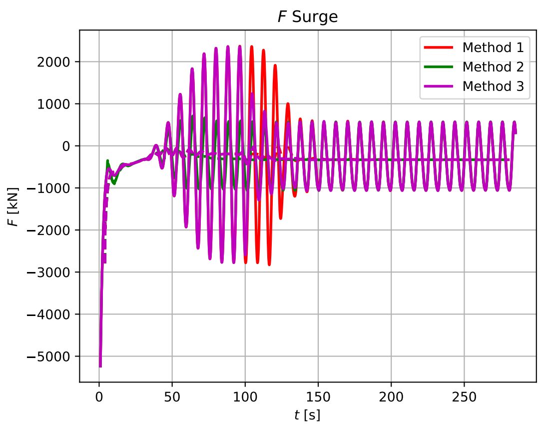

(a)

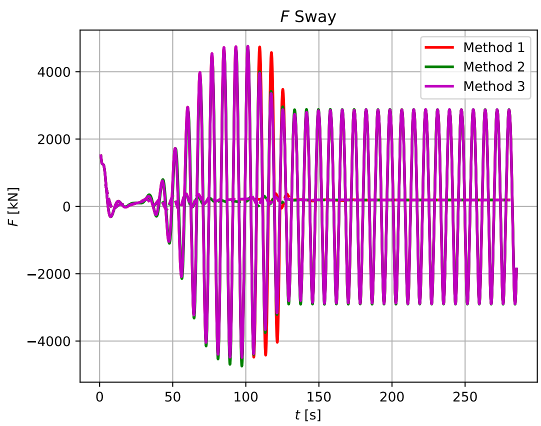

(b)

Figure 4.14: *Time traces of the forces in surge (a) and sway (b) for a sailing ship with 4DoF.*

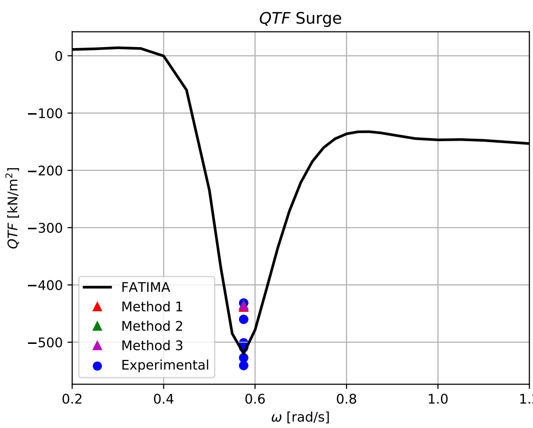

(a) *$QTFx$*

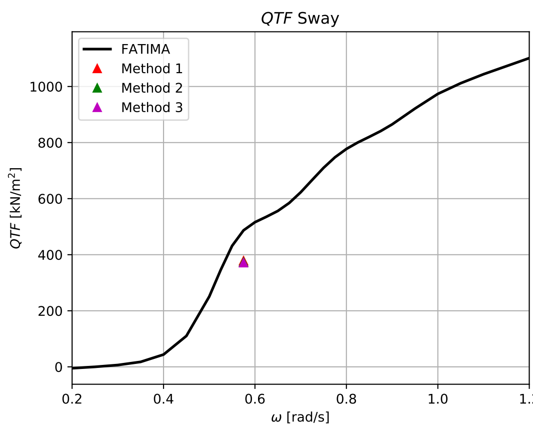

(b) *$QTFy$*

Figure 4.15: *QTF of surge (a) and sway (b) as a function of frequency for a sailing ship with 4DoF.*

4.2.3 4DoF (heave, roll, pitch and yaw) and 5DoF (sway, heave, roll, pitch and yaw)

Then a 4DoF simulation with yaw instead of sway is ran, as well as a 5DoF simulation with both yaw and sway. The results from these configurations are also compared to the 4DoF with sway simulation, to more easily see the influence of setting sway free.

The time traces of the motions for these simulations are shown in Figure 4.16. In Figure 4.16a it stands out that the drift for sway in the 5DoF case is significantly higher than it was in the 4DoF case. The reason for this is that the yaw and sway strongly impact each other, thus yaw being free significantly changes the sway force on the ship. As a result the spring coefficient is less accurate in the 5DoF case, resulting in a larger drift. However, considering it is only a drift of 2 meters over a duration of 2 minutes for a ship of over 30 m breadth, this is not expected to impact the force response significantly.

Figure 4.16b shows the yaw motion time trace. Note that because only a small deviation in yaw angle is allowed by the spring model, there is no need to give the ship an initial rotation. Here it can be seen that both cases reach a reasonably stable state in a similar amount of time. However, the stable state for the 4DoF case is for a slightly higher yaw rotation compared to the 5DoF case. This means that the presence of sway also influences the yaw force response.

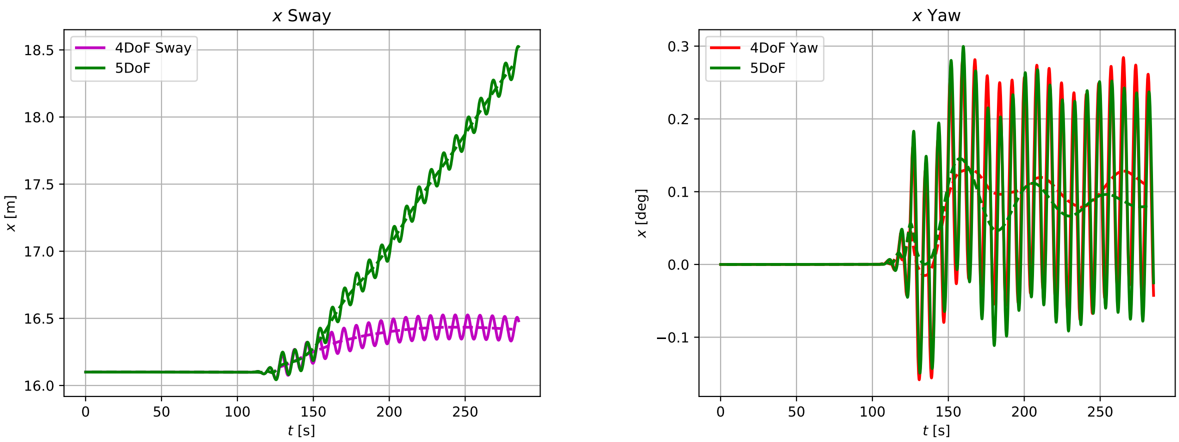

(a) (b)

Figure 4.16: *Time traces of the displacement of sway (a) and yaw (b) for a sailing ship with 4DoF and 5DoF.*

Figure 4.17 shows the *RAO* results for these three simulations. Here it is clear that both sway and yaw are well predicted compared to FATIMA and experimental results, in both the 4DoF and 5DoF simulations. However, 4.17c shows that for roll this is not the case. It turns out that the presence of yaw motion has a significant impact on the roll *RAO*. When yaw is fixed the roll motion is over-predicted. Conversely, the roll motion is slightly under-predicted when yaw is free, at least when comparing to experiments. The FATIMA and experimental results do not agree well here, and ReFRESCO looks to be an improvement over FATIMA at predicting roll motion.

Finally the force response, in terms of QTF, is given in Figure 4.18. The absence of experimental results makes it difficult to make conclusive statements about these values. However, FATIMA is meant to give an upper bound, and it is clear that for all simulations this is true. This gives a reason to be optimistic about these results. One problem is the disparity between the 4DoF and 5DoF results in the yaw QTF. This could be the result from an additional DoF, but it could also point to an error in the model. The 6DoF system will be used to find out whether that is the case.

4.2.4 6DoF

In this section the final DoF is added to the system, surge. This means that the ship is now free to translate and rotate in any direction. Initially the same wave frequency and wave amplitude as was used before is used to complete the methodology for a 6DoF system. Once a working methodology has been established, this is

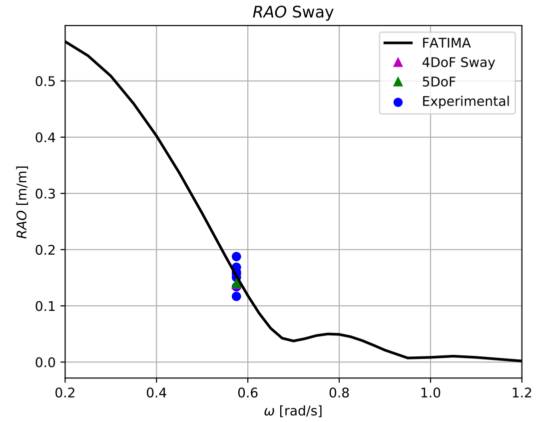

(a)

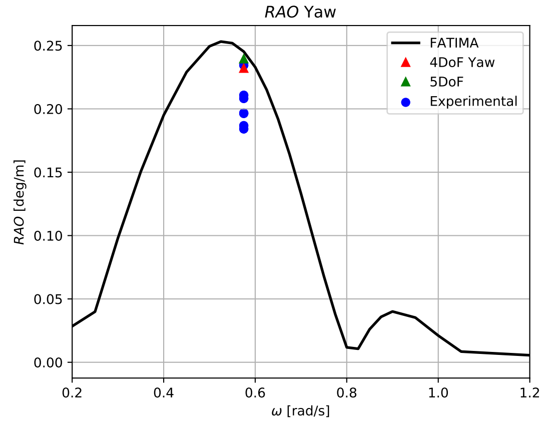

(b)

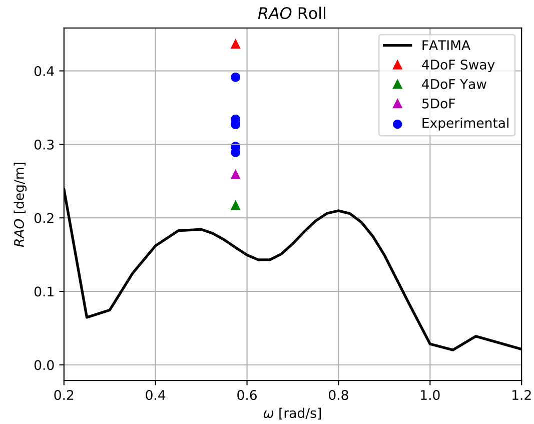

(c)

Figure 4.17: *RAO of sway (a), yaw (b) and roll (c) as a function of frequency for a sailing ship with 4DoF and 5DoF.*

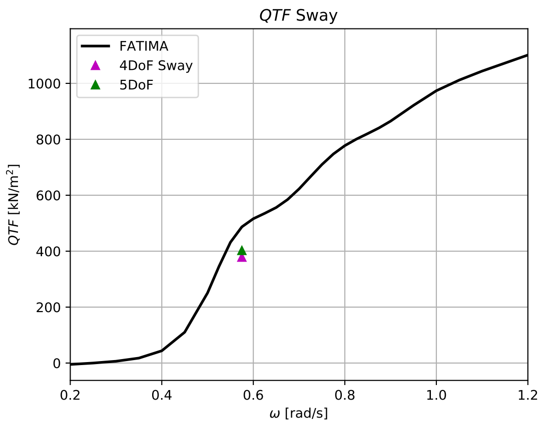

(a)

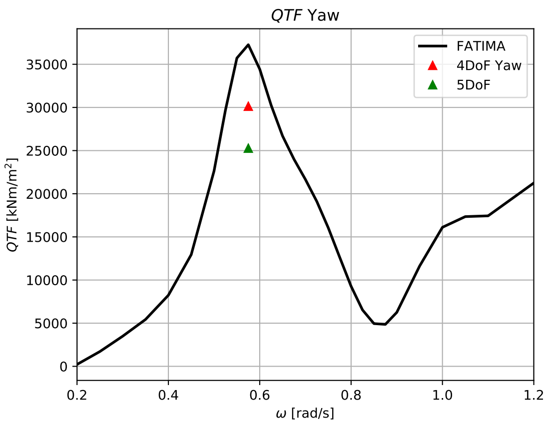

(b)

Figure 4.18: *QTF of sway (a) and yaw (b) as a function of frequency for a sailing ship with 4DoF and 5DoF.*

applied to a mesh convergence study as well as an investigation into the influence of the wave frequency and wave amplitude.

Initial workflow

For the 6DoF a more general method is employed to create the simulations. A workflow is formulated in such a way that it can be used without running the lower DoF simulations first. First a calm water simulation in 2DoF is done to find non-physical values for F_y, M_x and M_z. These forces are countered in the 6DoF system by use of an external force. The same is done with the calm water result for F_x.

Then a simulation with waves is done for about ten fully developed waves. This allows us to accurately determine the wave amplitude in the simulation. The wave amplitude that the ship is affected by is not the same as the wave amplitude that is given as an input, due to wave deprecation. The wave amplitude is then used together with the QTF solutions from FATIMA to find an approximation for the stiffness constants of the springs using the initial spring method. Assuming that the FATIMA results are reasonably close to the CFD results, this should give a good approximation on the spring constants.

The spring constants for Simulation 1 in the upcoming results have been defined using this workflow . The springs in Simulation 2 through 4 are defined iteratively, based on the mean force of the previous simulation. That is, the spring constant of Simulation i is equal to the mean wave added resistance in Simulation i-1 divided by the chosen x_0. Here i runs from 2 to 4. The stiffness constant for the spring in yaw is kept constant.

The result in terms of the motion time traces is given in Figure 4.19, while the corresponding RAO results are presented in Figure 4.20. From these figures it can be seen that hydrodynamically in all cases, the solution is expected to work reasonably well. Even a movement of 10 m is less than 10 % of the L_{PP}. As such, the force response is expected to be consistent between the simulations. This is visible in the RAO response, which matches reasonably well for all four simulations. Though, it does turn out that the roll motion consistently decreases for lower values of sway drift.

However, as can be seen in Figure 4.21 where the force response of the ship is plotted, there is a significant difference in the resulting F_y and M_z. Again it can be seen that lower values of sway drift have a large influence. This is in part of course because the yaw angle is different, and thus the forces on the ship also. However, the difference between the yaw angles is a fraction of a degree, and should not have such a large influence on the QTF. From these results it can also be seen that the spread of the QTF results is correlated with the sway velocity. In particular, is looks as though higher sway velocities correspond to higher values for the QTF for both sway and yaw.

Other spring models

To alleviate the influence of the sway velocity on the force response three new simulations are defined using different spring models defined in the method section. Simulation 1 uses the single RAO model in surge, sway and heave without pretension. Simulation 2 is the same as simulation 1, but does use a pretension is all three directions. Simulation 3 uses the double RAO model with pretension for surge and sway and the rudder model for yaw.

The idea here is that the ship deviates significantly less from its stable position compared to the initial spring model, since the spring constants are significantly higher. This ensures that the drift velocity is close to zero and as such does not disturb the force response significantly. Moreover, with low drift velocity all models are expected to give essentially the same results. By using multiple models, the influence of small changes can easily be seen.

The result is given in Figure 4.22. Here it can be seen that, despite the mean of the displacement of the free motions being insignificantly small compared to the size of the KCS, it still has a massive influence on the force response, in particular the QTF of yaw. The drift velocity is so low in these simulations that it can not be responsible for the differences between the results of the different models.

Instead, these issues could be the result of numerical problems, in particular of the mesh. The iterations with a higher displacement in sway and yaw correspond to higher values of the QTF. Therefore it is possible that the non-physical force that was found in the calm water simulation during the 2DoF simulation is not a constant force, but is highly dependent on the position of the ship. This idea is strengthened by the behaviour of the QTF of surge, for which there is almost no difference between the simulations. Since the grid is much better defined in this direction than in the sway direction lower non-physical errors due to deformation are expected here, which is the case.

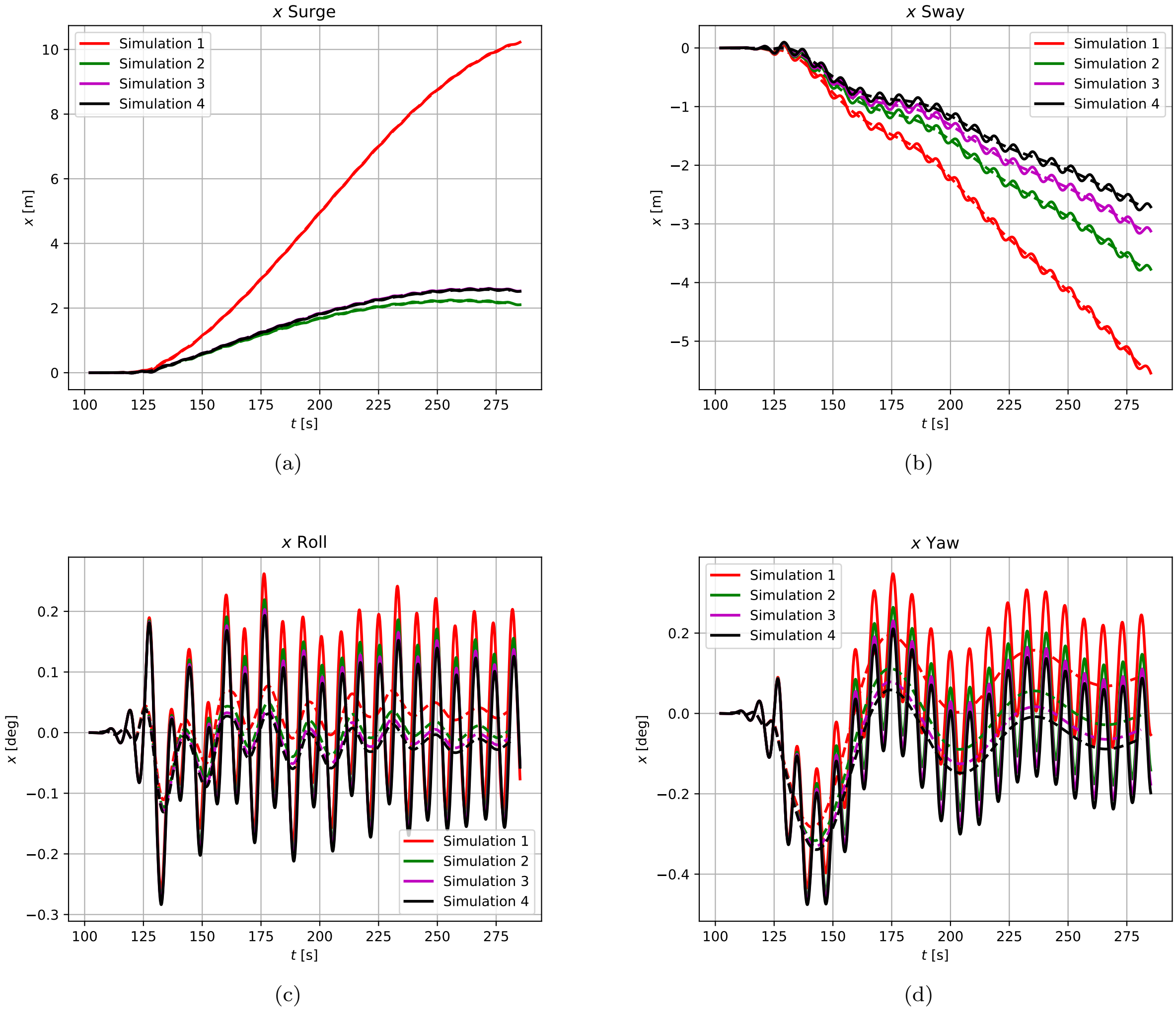

Figure 4.19: *Time trace of the displacement of surge (a), sway (b), roll (c) and yaw (d) in a 6DoF system.*

To test this hypothesis the three simulations shown in Figure 4.22 are used once more. After each of these simulations the mean position of the ship over the last 8 wave periods is calculated. Then new calm water simulations are made where the ship is placed at the calculated position. This calm water simulation uses the same mesh, so the mesh deformation happens in the same way compared to the full simulations shown in Figure 4.22. These calm water simulations are done with a captive ship, meaning that the ship has 0DoF, and the resulting forces at these position of the ship are noted for surge, sway and yaw.

The results are given in Figure 4.23. In this graph the force response in sway and yaw is given for all three simulations both in the full simulation and in the captive calm water simulation. Here it is clear that there are significant differences in the non-physical forces of the simulations, despite all using the same mesh. This means that the position of the ship in the mesh has an enormous effect on the magnitude of the non-physical force, as the calm water contribution is very low since the yaw angle is very low.

To check whether this non-physical force is the reason for the difference in QTF, Equation 4.1 is used. This equation is based on Equation 2.11 from the theory section and essentially divides the total force contribution into the force contribution due to the waves, the calm water and the non-physical force due the mesh. The wave simulations shown in Figure 4.22 were influenced by all three contributions, thus the force measured there was equal to the total force. Conversely, the captive simulations did not have waves, and thus only had contributions of the mesh and the calm water. Equation 4.1 thus clearly shows that to find the wave added resistance one needs to simply take the difference between the wave simulation and the corresponding captive

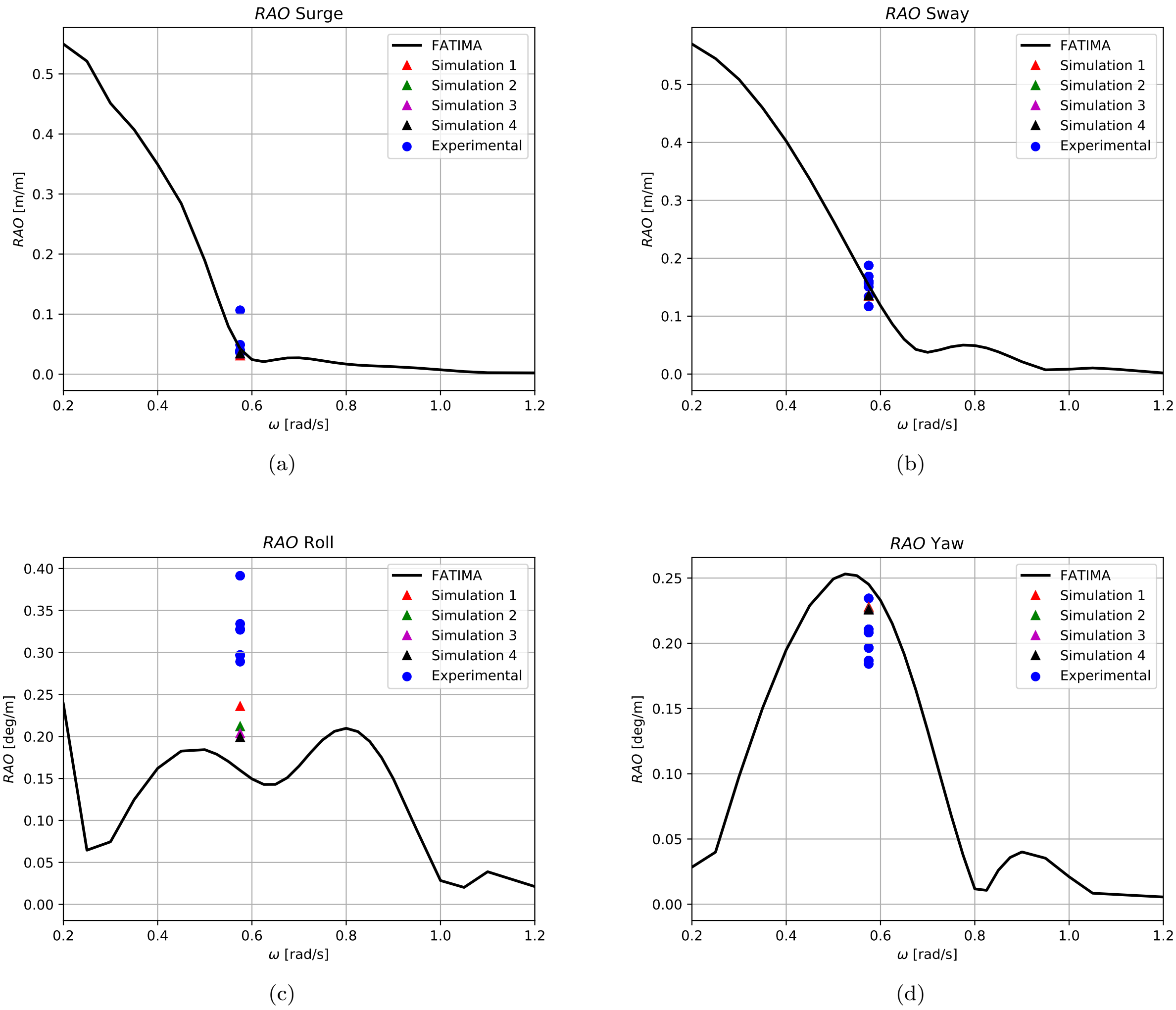

Figure 4.20: *RAO of surge (a), sway (b), roll (c) and yaw (d) as a function of frequency in a 6DoF system.*

simulation.

$$\overline{F}_{\text{Total}} = \overline{F}_{\text{Waves}} + F_{\text{CW}} + F_{\text{Mesh}} \tag{4.1}$$

The result is also shown in Figure 4.23. There it is clear that after taking the difference, the force response of the three simulations are very similar. This can also be seen when using these results to calculate the QTF, as is shown in Figure 4.24. Now that the captive simulation is taken into account in the calculation for the QTF, the differences between the methods becomes small. The differences that are still there are most likely due to the non-linearity of the non-physical force contribution, as the force is only calculated at a mean position. However, this error is only minor in this case. However, it is possible that a different mesh leads to a larger error.

Conclusion

A methodology has now been found that works reasonably well for a single specific case in a 6DoF system and is expected to work for the other cases as well. The results are gathered by running a captive calm water simulation after the regular simulation in waves to find the contribution of non-physical forces on the ship due to the mesh deformation. The results from the simulation in waves are then corrected for these forces. Note that it is not needed to correct for the non-physical force contribution during the simulation when using this method, only during the analysis.

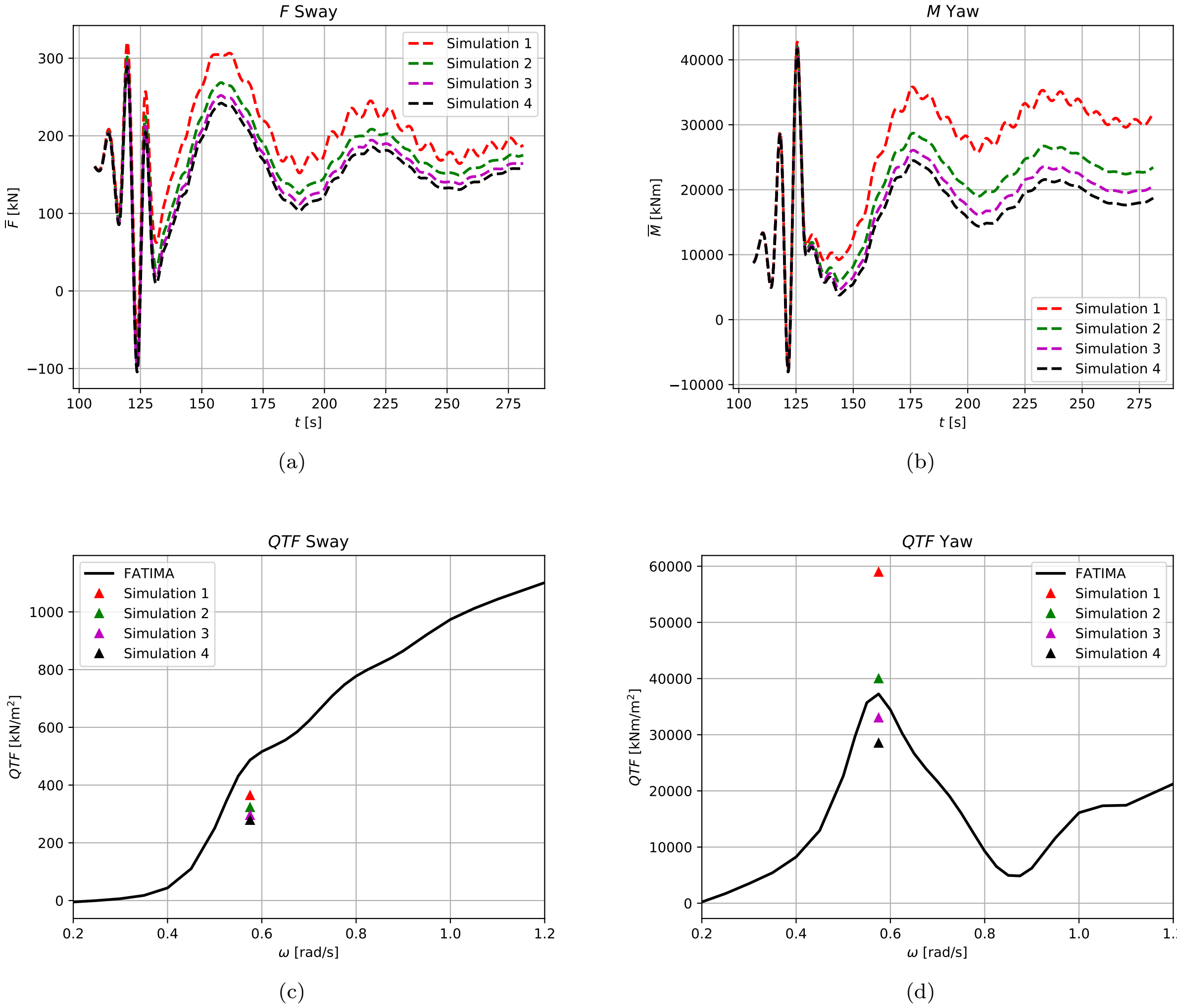

Figure 4.21: *Time traces of the moving average of the sway force (a) and the yaw moment (b), and the corresponding sway (c) and yaw (d) QTF as a function of frequency in a 6DoF system.*

Now that the error on the numerics has been found, one could conclude that the measures taken to limit the drift are no longer necessary. However, since the captive simulation is based on a mean position this method is most accurate when the ship stays as close to the mean position as possible. This means that for lower drift the non-physical forces of the captive simulation are a more accurate measure of those in the simulation in waves. Therefore the methods that were found before, meant to limit the drift and drift velocity, are still kept as an essential part of the methodology.

4.2.5 Mesh convergence

Now that a methodology for a ship with 6DoF is found a mesh convergence study is done. Here three different meshes are used. The coarse mesh is the same mesh that was used previously while developing the 6DoF methodology. The finer and finest mesh have 1.5 and 2 times the amount of cells the coarse mesh has in the mesh initialization step of the meshing strategy, respectively. The rest of the strategy is exactly the same, though some refinement levels are changed slightly to ensure the constraints on the orthogonality and equiangular skewness are satisfied. Moreover, the number of time steps per wave period is changed to account for the decrease in cell size.

The results in terms of RAO and QTF are shown in Figures 4.25 and 4.26, respectively. Here it is clear that, while the results of the coarse mesh and the finer meshes are not exactly the same, the differences are

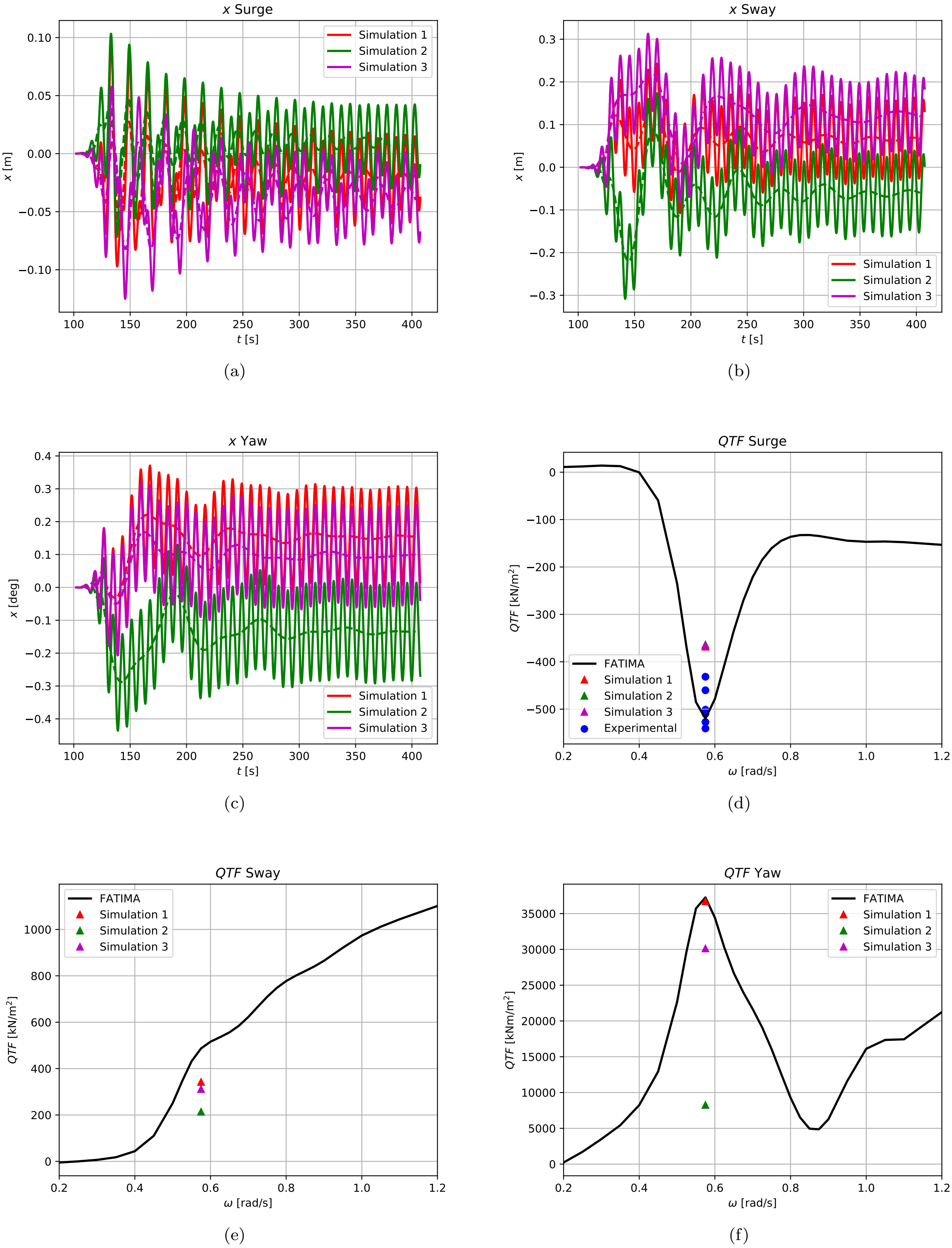

Figure 4.22: *Time traces of the displacement of surge (a), sway(b) and yaw(c), and the QTF of surge (d), sway(e) and yaw (f) as a function of frequency for a ship sailing with 6DoF.*

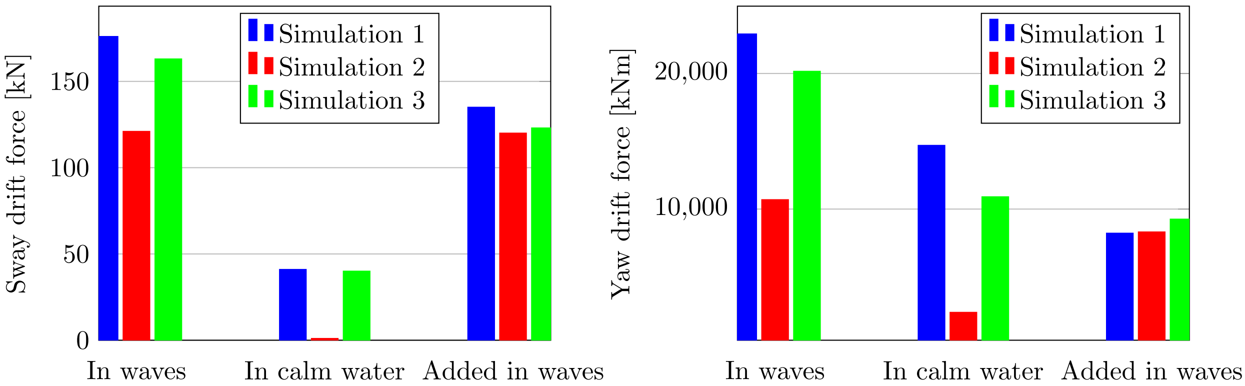

Figure 4.23: *Sway and yaw force in the total simulation, the captive simulation and the difference between these forces for the three simulations.*

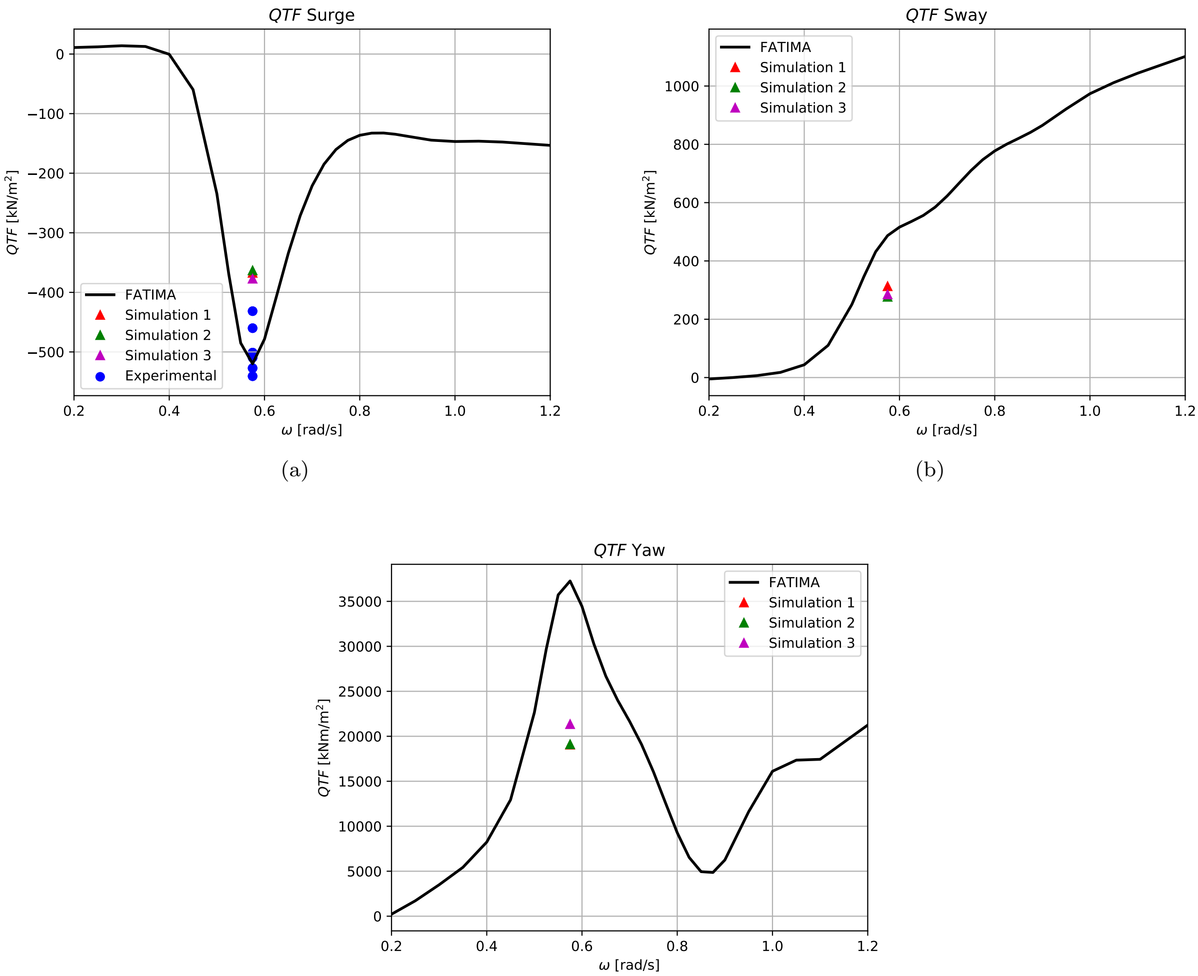

(a)

(b)

(c)

Figure 4.24: *QTF of surge (a), sway(b) and yaw (c) as a function of frequency in a 6DoF system.*

relatively small. As a result it is concluded that the coarse mesh does a reasonable job at predicting the ship response.

Moreover, it shows that for some of the DoFs for which ReFRESCO slightly underpredicted the result compared to FATIMA and experimental work, this under-prediction was caused by the mesh. For instance heave is slightly under-predicted by ReFRESCO when using a coarse mesh, but when using the finer meshes the experimental value and the CFD results closely match.

Another interesting conclusion that can be made here is that the coarse mesh is good enough to get proper results for the QTF values, despite only considering the average of the non-physical forces. While the QTF of surge is under-predicted by ReFRESCO, this is the case for both the fine meshes and the coarse mesh and is thus inherent to the methodology. For the QTF of sway and yaw it is hard to say whether the CFD properly predicts the results, since the FATIMA results just give an upper bound. However, it can be seen that the mesh dependence for sway is minor. For yaw the mesh dependence is significantly larger, though the results are in the same magnitude. The difference in the meshes is most likely caused by the error in the location of the captive simulation, as the force contribution in yaw due to this effect is significant and the RAO values are correctly predicted.

4.2.6 Bow Quartering Frequency Range

Now that the methodology is working for the considered frequency and amplitude, it is applied to the frequencies mentioned in the methodology section. The result in terms of the RAO is given in Figure 4.25. Here it can be seen that for most of the motions, the CFD results match closely with the experimental and FATIMA results. One interesting observation that can be made is that both heave and pitch, shown in 4.25c and 4.25e respectively, agrees very well with FATIMA for the high frequency results but less so for the low frequency results. The most probable cause of this is that the mesh is too coarse, as the mesh dependence study showed that finer meshes do a better job at predicting these motions. The underprediction is only marginal though, and the results are quite close to experimental values.

The biggest outlier though, is the roll RAO. While the CFD results follow a similar pattern as the FATIMA results, the values are quite far off. However, this does not immediately mean that there is a problem with the CFD. The CFD results actually compare better to experiments than FATIMA does. Moreover, there is quite a large variation in the experimental results as well, which could explain the difficulty of predicting roll, as it means that it is very sensitive to small changes.

The results in terms of the QTF are given in Figure 4.26. In Figure 4.26a it is clear that the ReFRESCO and experimental results are fairly close. This is important, as this indicates that ReFRESCO does a good job at predicting the force response of the ship.

For sway and yaw it is more difficult to validate the CFD results, as there are no experimental results. Looking at 4.26b and 4.26c, it might seem as though the FATIMA and ReFRESCO results disagree with one another, as the results differ significantly. However, it is also clear that in both cases the trend is very similar. Moreover, it is important to keep in mind that the assumptions for FATIMA make it more of an upper bound to the real value than a good approximation. Since the CFD always predicts value below FATIMA, or very little above it, it is entirely possible that the CFD prediction is close to the real situation.

While a conclusive argument on the accuracy of the sway and yaw QTF cannot be made based solely on this data, it still gives a good initial data set. No investigations into these QTF values were found in literature as of yet, but with the recent increase of popularity of CFD in the seakeeping community more investigations into the QTF using other programs will hopefully be done in the future. For those investigations the results presented here could be used for comparison and validation.

4.2.7 Bow Quartering Amplitude Range

The RAO and QTF are designed such that the response in terms of these parameters is independent of the wave amplitude. In this section a number of cases with different wave amplitudes were simulated for a single frequency to verify this.

The results in terms of the RAO and the QTF are shown in Figures 4.27 and 4.28, respectively. Here the FATIMA result is plotted as a dashed line for clarity, since FATIMA uses an infinitesimally small wave amplitude in its calculations. Here it is clear that for most of the RAO and QTF values the independence of the amplitude is present as expected.

However, there are two results that stand out: the RAO of roll and the QTF of yaw, depicted in Figures 4.27d and 4.28c. For roll it can be seen that a higher wave amplitude leads to a marginally higher RAO value. This is not something that was expected, nor is it visible in the experimental results. The reason for this behaviour was not found during this study.

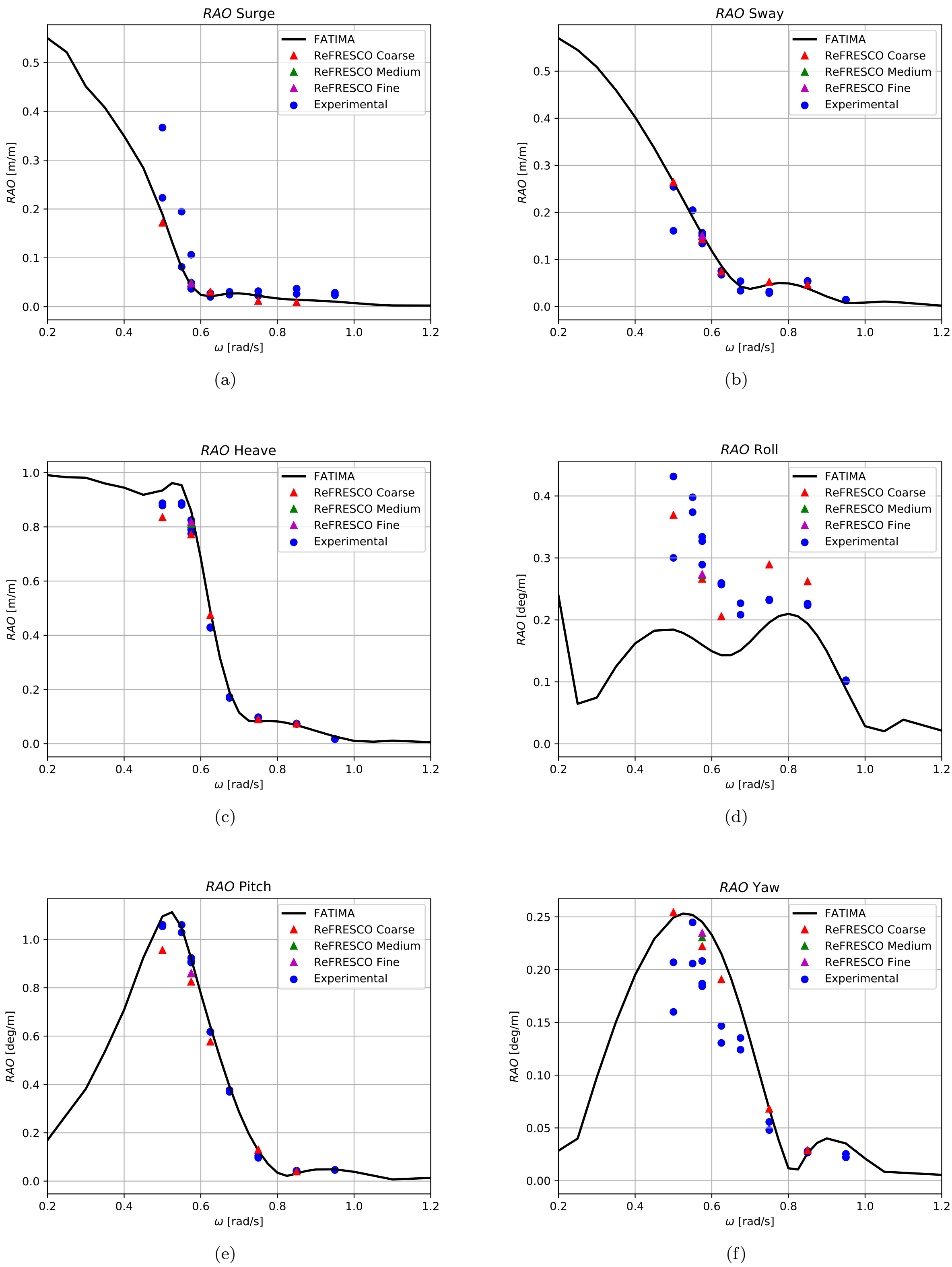

Figure 4.25: *RAO of surge (a), sway (b), heave (c), roll(d), pitch(e) and yaw(f) as a function of frequency in a 6DoF system.*

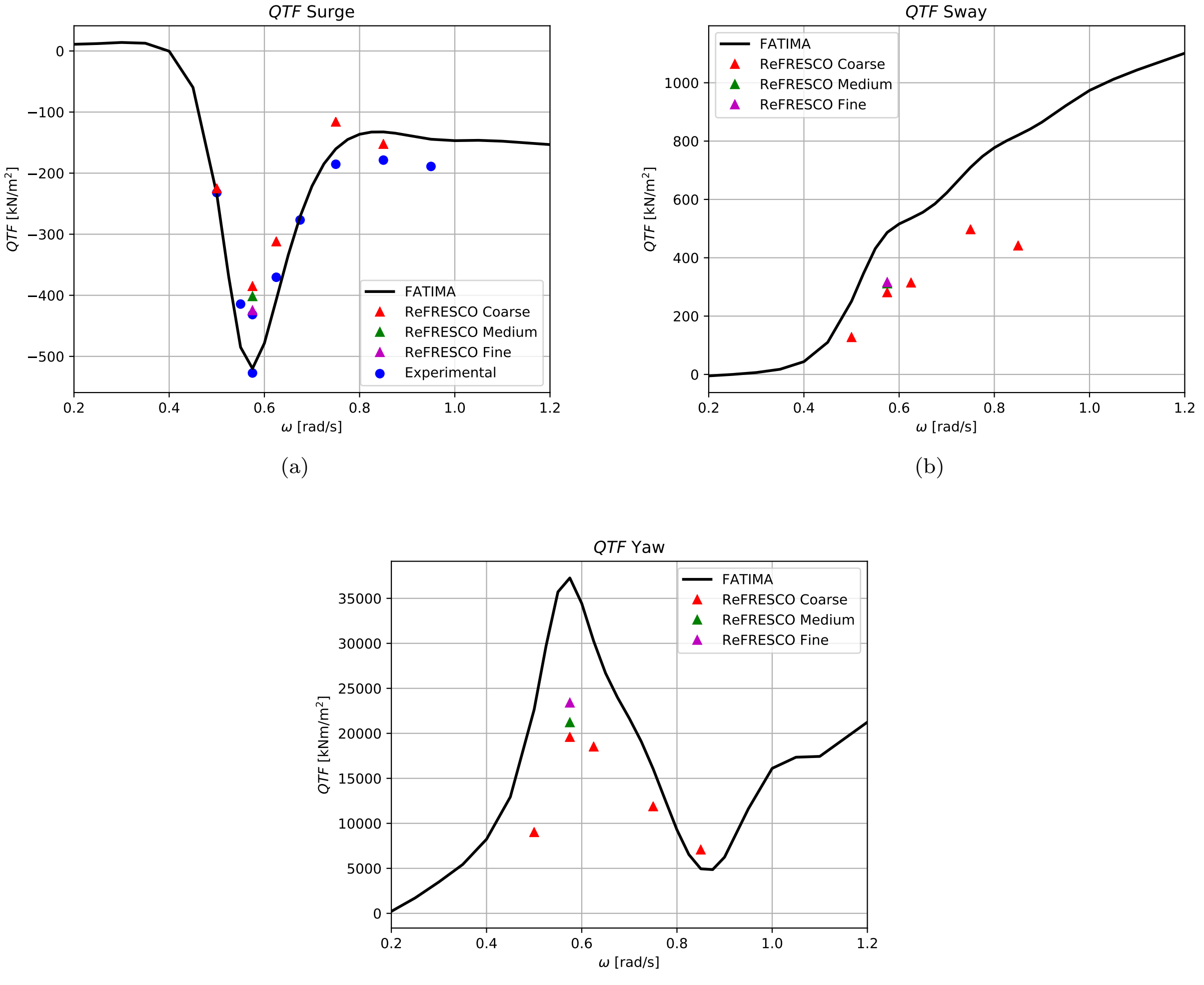

(a) (b) (c)

Figure 4.26: *QTF of surge (a), sway (b) and yaw(c) as a function of frequency in a 6DoF system.*

For the QTF of yaw there is no experimental comparison available, so it is impossible to say if this amplitude dependency is realistic or not. This would have to be found out through more detailed investigations into the QTF of yaw specifically.

4.3 Stern quartering waves

Now the heading is changed from bow quartering waves to stern quartering waves. The same methodology that was applied for the 6DoF in bow quartering is immediately applied here. The only difference is that a roll damping factor is used, equal to 10% of the critical damping. The reason this is done is that this factor was used in the generation of the FATIMA results as well.

4.3.1 Mesh convergence

The first thing to consider in stern quartering is the mesh convergence. This is done in a similar way as was done for bow quartering. In this case the meshes have 1, 1.33 and 1.5 times the initial number of cells. The results are shown in Figures 4.29 and 4.30 for the RAO and QTF results, respectively. In these figures the results of varying frequency is also shown.

When considering the RAO results it can be concluded that the mesh is properly converged. There are some differences between the meshes for some of the parameters, especially sway and yaw, but these are only

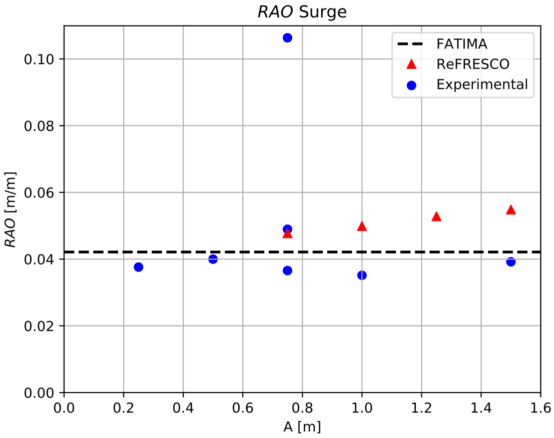

(a)

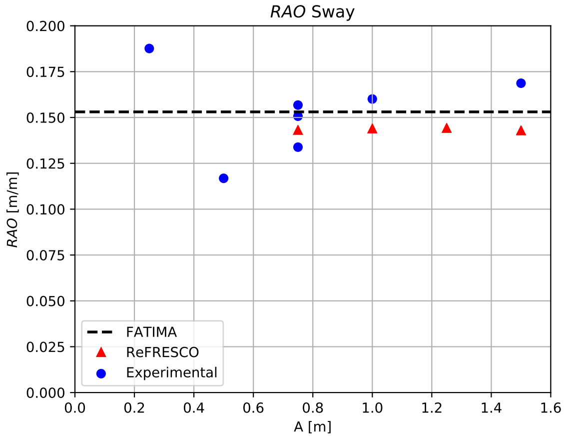

(b)

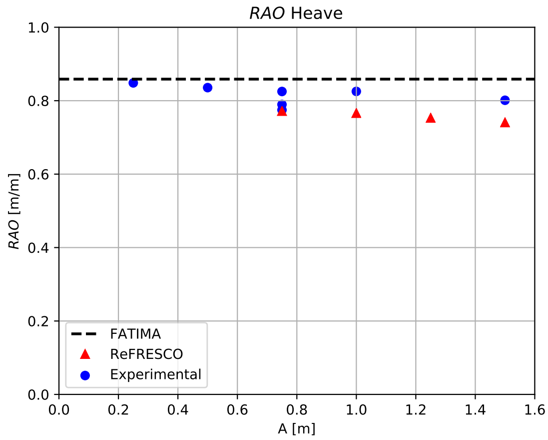

(c)

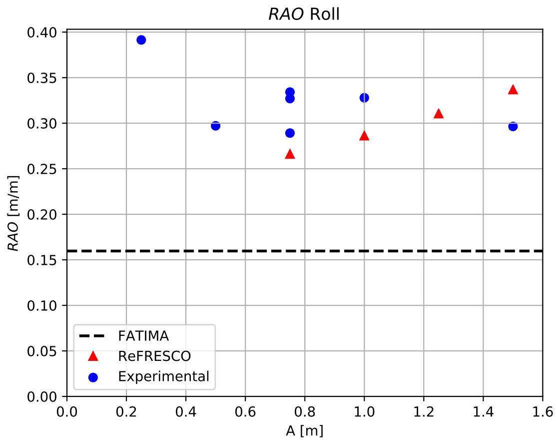

(d)

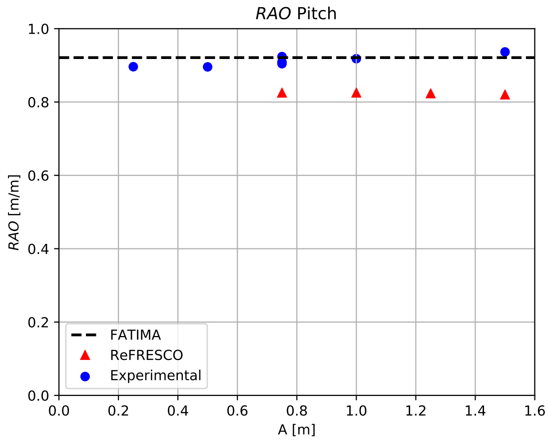

(e)

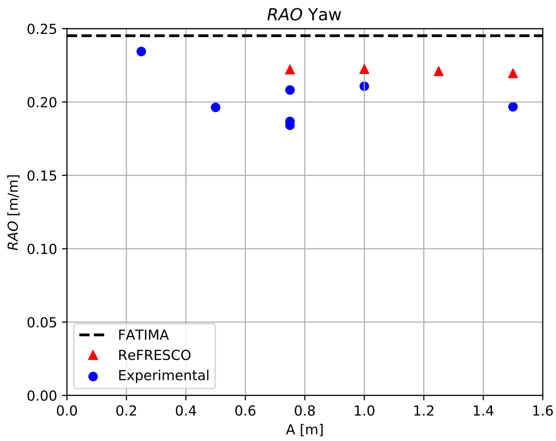

(f)

Figure 4.27: *RAO of surge (a), sway (b), heave (c), roll(d), pitch(e) and yaw(f) as a function of amplitude in a 6DoF system.*

minor. As a result, the motion response of the ship in stern quartering seas is said to be mesh independent.

For the force response this is not the case. For the QTF of surge the differences are relatively minor. They

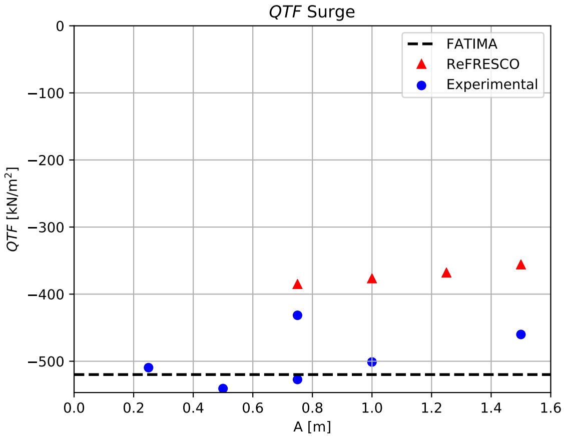

(a)

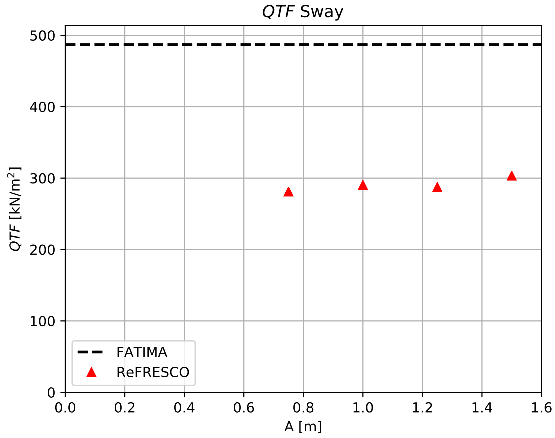

(b)

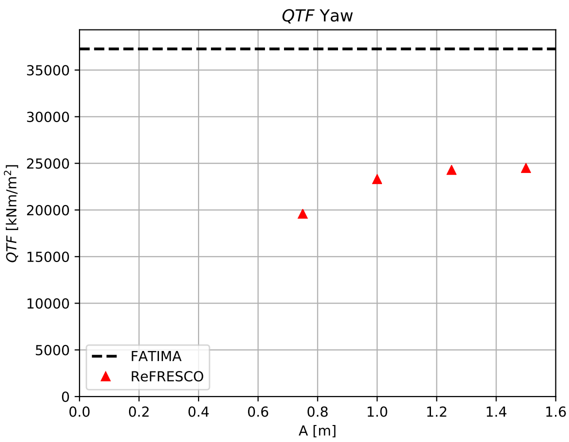

(c)

Figure 4.28: *QTF of surge (a), sway (b) and yaw(c) as a function of amplitude in a 6DoF system.*

are too big for the results to be called completely mesh independent, but they do prove that even with a coarse mesh a reasonably approximation can be achieved, as the different meshes do give similar results. Given that the goal for this study was to find a fast and rough solution, this error is not necessarily a big issue for this purpose.

For the QTF of sway and yaw the issue is larger. The difference between the fine and the medium mesh is significant. The questions thus comes up whether an even finer mesh would give a significantly different result. This is hard to predict, making the results for the QTF of sway and yaw unreliable.

As a result it is important to consider where the error comes from. The most likely reason is that the motion response for stern quartering is much stronger than for bow quartering, as can be seen from the higher RAO values. As a result, a larger error is introduced in the captive simulation, as that only takes into account the mean position of the ship and not the ships deviation from this position. Any non-linearity in the non-physical force contribution is thus stronger in the stern quartering QTF results than in the bow quartering results.

Since the RAO values are well predicted, when comparing to experiments, this non-linearity is the most likely source of the error. Improving the method for determining this non-physical force contribution thus results in a decrease of the error in the QTF.

4.3.2 Frequency range

Now that the mesh independence is ensured, a number of simulations with different wave frequencies are considered. This is again done using the coarse mesh.

The results in terms of the RAO and QTF are presented in Figures 4.29 and 4.30. Here it is clear that the motions match the FATIMA results reasonably well for all cases apart from roll, for which the CFD value significantly over-predicts compared to FATIMA and experiments. It is difficult to say where this problem comes from with the available data.

In Figure 4.30a it is clear that the QTF of surge is reasonably well predicted compared to FATIMA and experiments. The QTF of yaw and sway are more difficult to compare, since there are no experimental results to compare to. However, the trend line that is seen is comparable to the trend line in FATIMA, which is promising.

Here it should be noted that, based on the mesh convergence study, there are significant errors present in these QTF values due to the non-physical force. However, since the same mesh is used for all frequencies and the drift is low, the non-physical force is expected to be of similar magnitude in all cases. This means that the trend line still gives valuable information despite the errors caused by the mesh.

4.3.3 Amplitude range

The results in terms of the RAO and QTF are presented in Figures 4.31 and 4.32. Here it is clear that most results are indeed independent of the amplitude, as expected. However, the RAO of sway and the QTF of sway and yaw are not. These are interesting and unexpected observations, especially when considering that this was not the case for bow quartering. Further investigations could be aimed at investigating where this comes from, and if this is true for all amplitudes or only for a certain range of amplitudes.

What is also interesting is that it looks as though the sway RAO results from FATIMA and CFD agree very well for infinitesimally small amplitudes, when extrapolating the CFD results. Given that for the other frequencies the sway is slightly under-predicted compared to FATIMA, it is possible that the amplitude dependence is inverted for these cases. Where this behaviour comes from is not yet clear.

For the QTF of sway and yaw the same mesh is used for all three cases. However, the non-physical force contribution is not expected to be the same in this case. The reason for this is that larger amplitudes lead to large oscillations of the motion and thus a larger deviation from the ship mean position. This is taking into account when calculating the RAO and QTF, but still has an effect on the non-physical force. It is possible that this is responsible for the non-linearity of the sway and yaw QTF, but it cannot be said with certainty from these results.

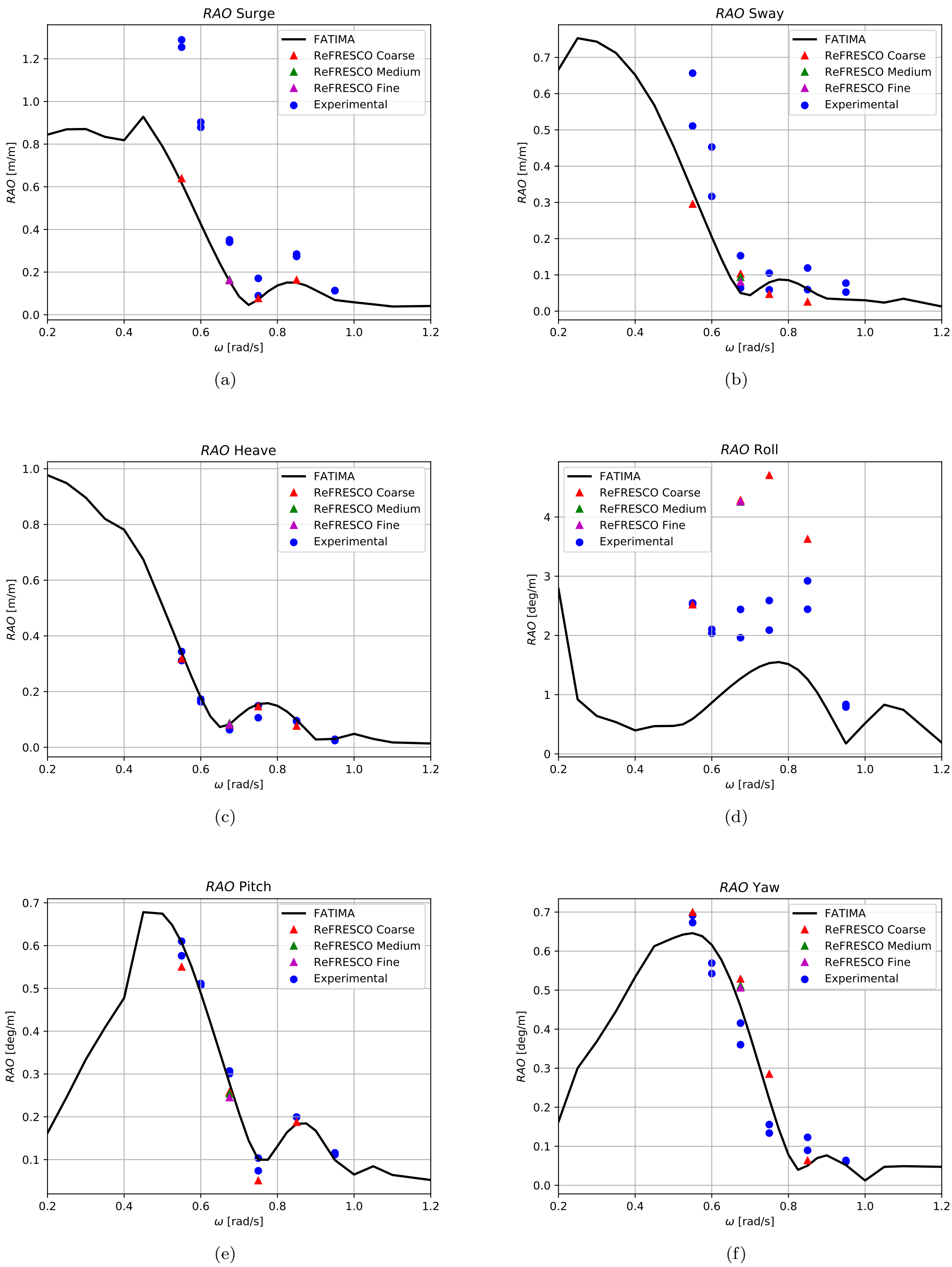

Figure 4.29: *RAO of surge (a), sway (b), heave (c), roll(d), pitch(e) and yaw(f) as a function of frequency in a 6DoF system. The results of the mesh convergence study is also depicted.*

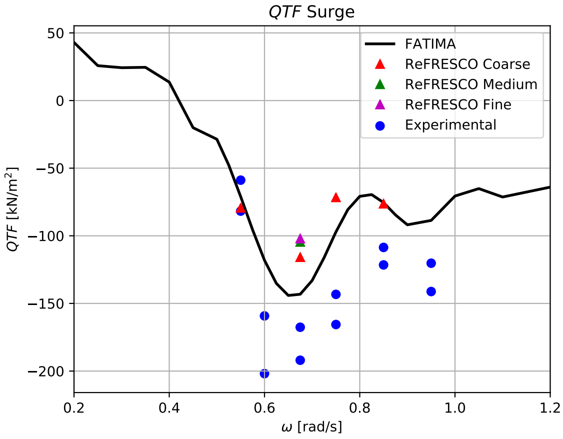

(a)

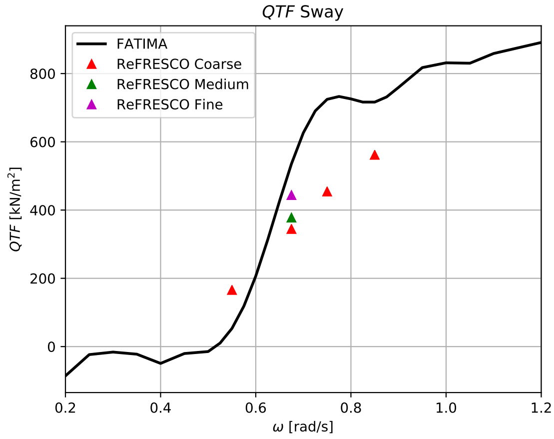

(b)

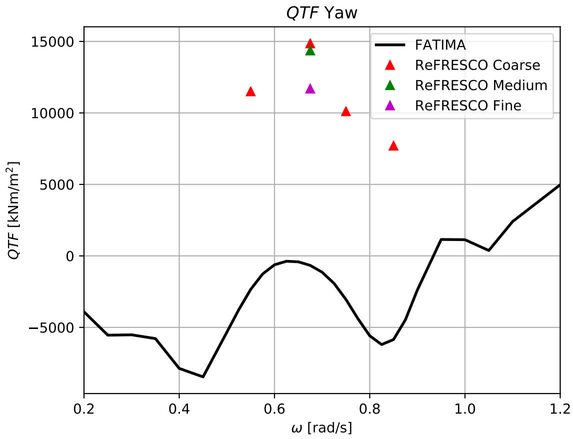

(c)

Figure 4.30: *QTF of surge (a), sway (b) and yaw(c) as a function of frequency in a 6DoF system. The results of the mesh convergence study is also depicted.*

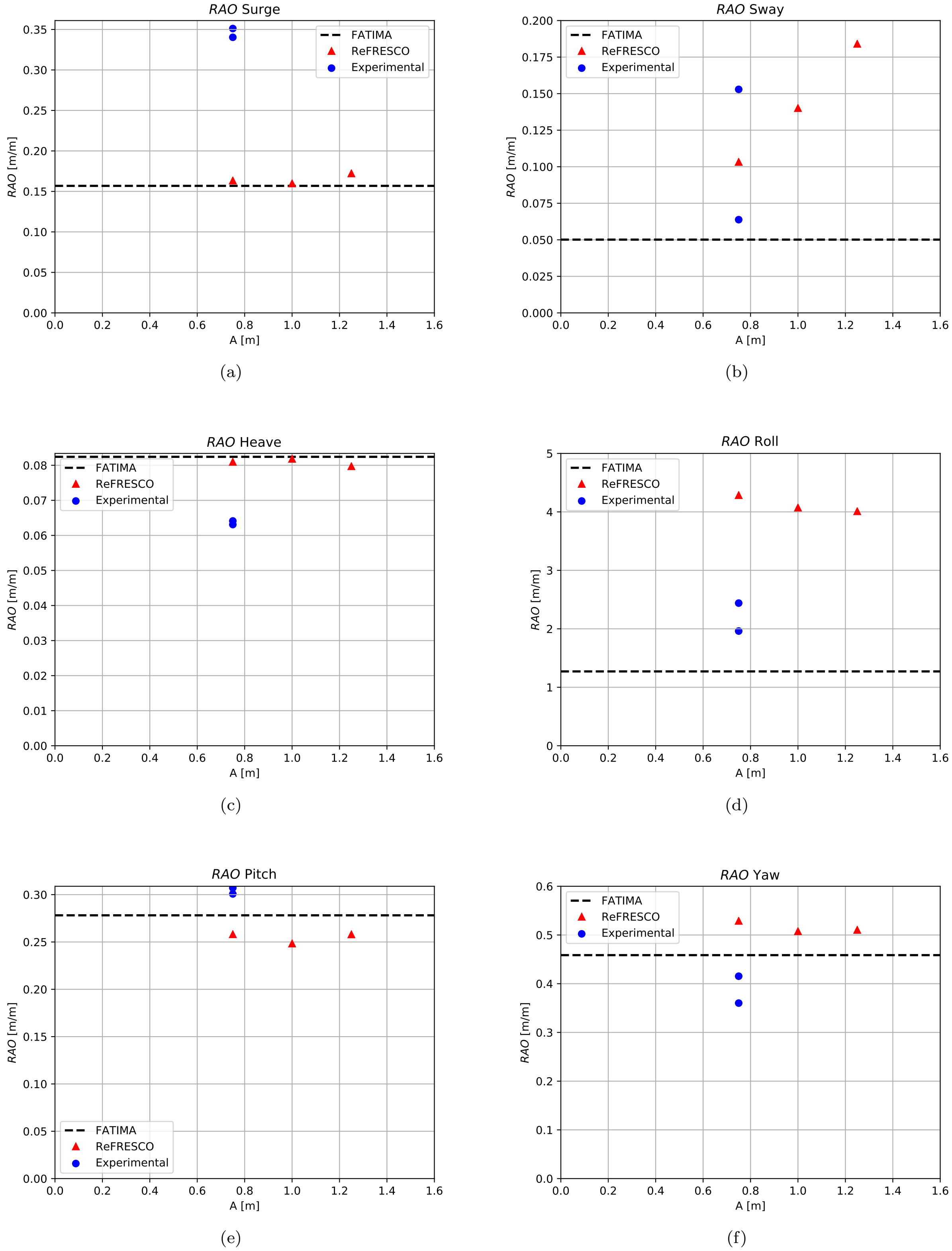

Figure 4.31: *RAO of surge (a), sway (b), heave (c), roll(d), pitch(e) and yaw(f) as a function of amplitude in a 6DoF system.*

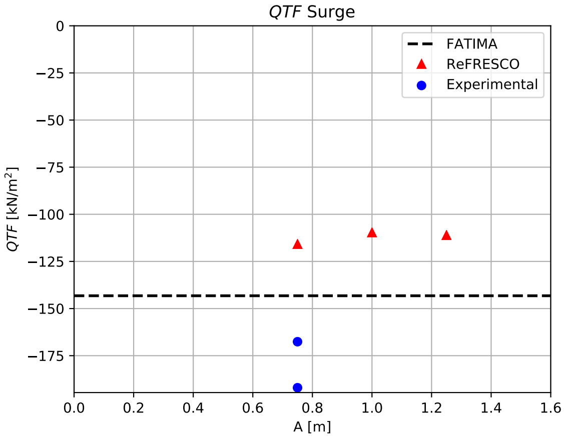

(a)

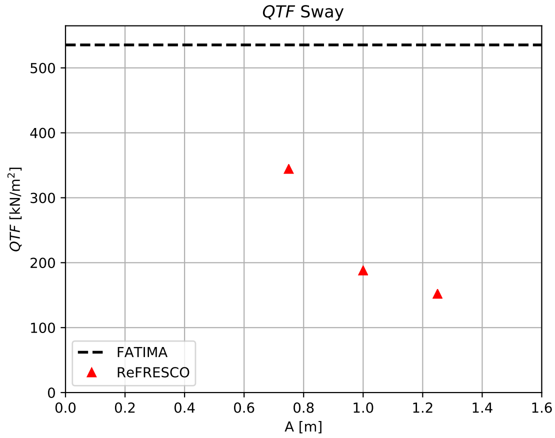

(b)

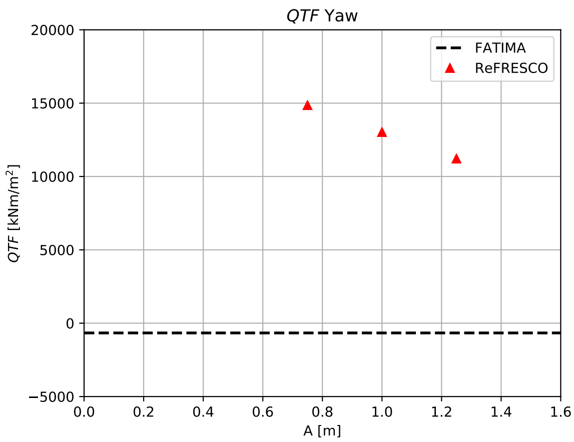

(c)

Figure 4.32: *QTF of surge (a), sway (b) and yaw(c) as a function of amplitude in a 6DoF system.*

5 Conclusions

In this report the methodology for simulating a sailing ship with 6DoF in quartering waves has been developed in ReFRESCO. To achieve a result in a timely manner, the choice was made to use a relatively coarse grid. Spring models were used to artificially create a stable position in the degrees of freedom where there is no physical restoring force. The spring coefficient was calculated such that drift is minimized, but the amplitude of the ship oscillations due to the waves were not impacted.

Using the springs, the motions of the ship in terms of RAO values showed good results when comparing to FATIMA and experiments. In order to isolate the wave added resistance from the total resistance, a fully captive calm water simulation was done to find both the non-physical contribution of the mesh as well as the calm water contribution on the forces at a mean position of the ship in the full simulation. By accounting for these influence when calculating the QTF values, different simulations using different spring models converge to a single result. For the QTF of surge this result showed reasonable comparison to experiments. For QTF of sway and yaw no experimental values are available and as such no conclusion about the validity of these results can be made.

Once a methodology was obtained, it was applied to a ship in waves of different frequency, amplitude, direction and mesh coarseness. Based on the mesh convergence studies it was concluded that even for a coarse mesh reasonable agreement between CFD, FATIMA and experiments was present. It was also found that roll is sensitive to change, and that it is difficult to make a conclusive argument about the accuracy of the roll predictions. Moreover, it was found that the RAO of roll was dependent on wave amplitude in bow quartering. Conversely, for stern quartering the RAO and QTF of sway as well as the QTF of yaw were dependent on amplitude.

6 Future Work

It would be beneficial if the non-physical force due to the mesh could be approximated more precisely, or could be minimized through a different method than is used in this study. This would result in an improvement over the results shown in this study, and perhaps could explain some or more of the unexpected phenomena that were seen in the results in this study.

Moreover, It would be interesting to do more research into the amplitude dependency of the RAO of sway and roll, and well as the QTF of sway and yaw. Finding out why and under which circumstances these parameters are amplitude dependent could be valuable to future research and to future comparisons between KCS results. This is especially true because the amplitude dependency is dependent on the heading.

It would also be interesting to do more research on QTF of yaw and sway. There is very little information to be found in literature on these subjects at the moment, because no experimental validation is possible. By investigating these values using different methods and programs, the validity of using this method in ReFRESCO to predict these values can be more accurately determined. It could also give valuable insights into possible limitations of this method.

Finally, the methodology in this work has been developed under rather strict limitations. It would be interesting to see how well this methodology holds up once these limitations are relaxed. For instance, the influence of using a different ship, irregular waves, putting the ship in shallow water or a ship standing still would be interesting to investigate.

References

[1] N. Salvesen, E. Tuck, and O. Faltinsen. Ship motions and sea loads (1970).

[2] J.-P. Boin, M. Guilbaud, M. Ba, et al. “Seakeeping computations using the ship motion Green’s function”. *The Tenth International Offshore and Polar Engineering Conference*. International Society of Offshore and Polar Engineers. 2000.

[3] H. Söding et al. A 3-D Rankine source seakeeping method. *Ship Technology Research* **56**.2 (2009), 50–68.

[4] S. P. Kim. CFD as a seakeeping tool for ship design. *International Journal of Naval Architecture and Ocean Engineering* **3**.1 (2011), 65–71.

[5] B. Guo, S. Steen, and G. Deng. Seakeeping prediction of KVLCC2 in head waves with RANS. *Applied Ocean Research* **35** (2012), 56–67.

[6] C. D. Simonsen et al. EFD and CFD for KCS heaving and pitching in regular head waves. *Journal of Marine Science and Technology* **18**.4 (2013), 435–459.

[7] V. Vukčević and H. Jasak. “Seakeeping validation and verification using decomposition model based on embedded free surface method”. *Proceedings, Tokyo 2015 Workshop on CFD in Ship Hydrodynamics*. National Maritime Research Institute. 2015, pp. 437–442.

[8] W. Kim, S. Van, and D. Kim. Measurement of flows around modern commercial ship models. *Experiments in fluids* **31**.5 (2001), 567–578.

[9] E. Ageno et al. A BOUNDARY ELEMENT METHOD FOR MOTIONS AND ADDED RESISTANCE OF SHIPS IN WAVES. *TRANSACTIONS OF FAMENA* **39**.2 (2015), 1.

[10] *MOERI Container Ship (KCS)*. URL: http://www.simman2008.dk/KCS/container.html.

[11] L. Davidson. *Fluid mechanics, turbulent flow and turbulence modeling*. June 2020. URL: http://www.tfd.chalmers.se/~lada/postscript_files/solids-and-fluids_turbulent-flow_turbulence-modelling.pdf.

[12] N. D. Katopodes. “Chapter 12 - Volume of Fluid Method”. *Free-Surface Flow*. Ed. by N. D. Katopodes. Butterworth-Heinemann, 2019, pp. 766–802. ISBN: 978-0-12-815485-4. DOI: https://doi.org/10.1016/B978-0-12-815485-4.00018-8. URL: http://www.sciencedirect.com/science/article/pii/B9780128154854000188.

[13] S. Sasic. *Multiphase flows Lecture 7*. 2019.

[14] *ReFRESCO*. URL: http://www.refresco.org.

[15] E. C. Tupper. “Chapter 9 - The Ship Environments”. *Introduction to Naval Architecture (Fifth Edition)*. Ed. by E. C. Tupper. Fifth Edition. Oxford: Butterworth-Heinemann, 2013, pp. 205–241. ISBN: 978-0-08-098237-3. DOI: https://doi.org/10.1016/B978-0-08-098237-3.00009-6. URL: http://www.sciencedirect.com/science/article/pii/B9780080982373000096.

[16] V. Bertram. *Practical ship hydrodynamics*. Elsevier, 2011.

[17] P. Crepier, S. Rapuc, and R. Dallinga. CFD Investigation into the Wave Added Resistance of Two Ships. *MARIN Internal Article* (2019).

[18] J. BOUGIS and E. N. S. DE MECANIQUE. ASYMPTOTIC STUDY OF THE WAVE FIELD GENERATED BY A STEADILY MOVING PULSATING SOURCE ().

[19] L. Bonfiglio, S. Brizzolara, and C. Chryssostomidis. Added mass and damping of oscillating bodies: a fully viscous numerical approach. *Recent Advances in Fluid Mechanics, Heat & Mass Transfer and Biology* (2011), 210–215.

[20] M. Alexandersson. A STUDY OF METHODS TO PREDICT ADDED RESISTANCE IN WAVES. *Master Thesis* (2009).

[21] J. M. Varela and C. G. Soares. “Interactive Simulation of Ship Motions in Random Seas based on Real Wave Spectra.” *GRAPP*. 2011, pp. 235–244.

[22] *HEXPRESS*. URL: https://www.numeca.com/en_eu/product/hexpress.

[23] S. Rapuc et al. Towards guidelines for consistent wave propagation in CFD simulations. *Proceedings of the 19th International Conference On Ship & Maritime Research (NAV), Trieste, Italy* (2018), 20–22.

[24] T. C. Rendall and C. B. Allen. Efficient mesh motion using radial basis functions with data reduction algorithms. *Journal of Computational Physics* **228**.17 (2009), 6231–6249.

[25] H. Schneekluth and V. Bertram. “Chapter 6 - Ship propulsion”. *Ship Design for Efficiency and Economy (Second edition)*. Ed. by H. Schneekluth and V. Bertram. Second edition. Oxford: Butterworth-Heinemann, 1998, pp. 180–205. ISBN: 978-0-7506-4133-3. DOI: https://doi.org/10.1016/B978-075064133-3/50006-2. URL: http://www.sciencedirect.com/science/article/pii/B9780750641333500062.

[26] R. Dallinga and R. Los-Elsenbroek. ACCURACY OF ADDED RESISTANCE EXPERIMENTS. Volume I: Test programme, set-up, measurements and analysis of the results. *MARIN Internal Report* (2018).

[27] T. H. Bunnik. Seakeeping calculations for ships, taking into account the non-linear steady waves. *Doctoral Thesis* (1999).